



**HAL**  
open science

## **Pb-free halide perovskites for solar cells, light-emitting diodes, and photocatalysts**

Pingping Jiang, Debdipto Acharya, George Volonakis, Marios Zacharias, Mikaël Kepenekian, Laurent Pedesseau, Claudine Katan, Jacky Even

### ► To cite this version:

Pingping Jiang, Debdipto Acharya, George Volonakis, Marios Zacharias, Mikaël Kepenekian, et al.. Pb-free halide perovskites for solar cells, light-emitting diodes, and photocatalysts. *APL Materials*, 2022, 10 (6), pp.060902. 10.1063/5.0095515 . hal-03694654

**HAL Id: hal-03694654**

**<https://hal.science/hal-03694654>**

Submitted on 13 Jun 2022

**HAL** is a multi-disciplinary open access archive for the deposit and dissemination of scientific research documents, whether they are published or not. The documents may come from teaching and research institutions in France or abroad, or from public or private research centers.

L'archive ouverte pluridisciplinaire **HAL**, est destinée au dépôt et à la diffusion de documents scientifiques de niveau recherche, publiés ou non, émanant des établissements d'enseignement et de recherche français ou étrangers, des laboratoires publics ou privés.

# Pb-free halide perovskites for solar cells, light-emitting diodes, and photocatalysts

Cite as: APL Mater. 10, 060902 (2022); <https://doi.org/10.1063/5.0095515>

Submitted: 11 April 2022 • Accepted: 19 May 2022 • Published Online: 10 June 2022

 Pingping Jiang, Debdipto Acharya,  George Volonakis, et al.

## COLLECTIONS

 This paper was selected as Featured



View Online



Export Citation



CrossMark

## ARTICLES YOU MAY BE INTERESTED IN

[Mechanism of Mn emission: Energy transfer vs charge transfer dynamics in Mn-doped quantum dots](#)

APL Materials 8, 020901 (2020); <https://doi.org/10.1063/1.5140888>

[Insights into the charge carrier dynamics in perovskite/Si tandem solar cells using transient photocurrent spectroscopy](#)

Applied Physics Letters 120, 173504 (2022); <https://doi.org/10.1063/5.0080109>

[Hydroxymethyl PEDOT microstructure-based electrodes for high-performance supercapacitors](#)

APL Materials 10, 061101 (2022); <https://doi.org/10.1063/5.0088452>

**APL Materials**

**Special Topic:** Design and Development of High Entropy Materials

Submit Today!



# Pb-free halide perovskites for solar cells, light-emitting diodes, and photocatalysts

Cite as: APL Mater. 10, 060902 (2022); doi: 10.1063/5.0095515

Submitted: 11 April 2022 • Accepted: 19 May 2022 •

Published Online: 10 June 2022



Pingping Jiang,<sup>1</sup>  Debdipto Acharya,<sup>1</sup>  George Volonakis,<sup>2</sup>  Marios Zacharias,<sup>1</sup>  Mikaël Kepenekian,<sup>2</sup>   
Laurent Pedesseau,<sup>1</sup>  Claudine Katan,<sup>2</sup>  and Jacky Even<sup>1,a)</sup> 

## AFFILIATIONS

<sup>1</sup>Univ Rennes, INSA Rennes, CNRS, Institut FOTON-UMR 6082, F-35000 Rennes, France

<sup>2</sup>Univ Rennes, ENSCR, INSA Rennes, CNRS, ISCR-UMR 6226, F-35000 Rennes, France

<sup>a)</sup>Author to whom correspondence should be addressed: [jacky.even@insa-rennes.fr](mailto:jacky.even@insa-rennes.fr)

## ABSTRACT

Metal halide perovskites have recently emerged as one of the most promising classes of semiconductors for various applications, especially in the field of optoelectronics. Lead-based halide perovskite materials, virtually unexploited for decades, have become prominent candidates due to their unique and intrinsic physicochemical and optical properties. Current challenges faced by the scientific community to capitalize on the properties of Pb-based perovskites are mainly associated with environmental concerns due to the toxicity of Pb and their poor stability. Under this context, over recent years, a number of new Pb-free halide perovskite (and perovskite-like) semiconductor classes have been introduced. This Perspective reviews recent developments in Pb-free halide perovskites, which specifically target their application in solar cells, light-emitting devices, and photocatalysts. Each type of Pb-free material is paired with a specific optoelectronic application, and the latest record performances are reported. Although these materials do not yet exhibit as attractive intrinsic optoelectronic properties as the Pb-based halide perovskites, their potential as alternatives for well-suited applications is discussed.

© 2022 Author(s). All article content, except where otherwise noted, is licensed under a Creative Commons Attribution (CC BY) license (<http://creativecommons.org/licenses/by/4.0/>). <https://doi.org/10.1063/5.0095515>

## I. INTRODUCTION

For the past decade, halide perovskite semiconductors have received tremendous attention due to their tunable bandgaps, impressive optoelectronic properties, ease of process, and low fabrication cost, all of which lead to an ever-expanding range of potential device applications.<sup>1</sup> This applies especially to their exploitation as solar cells, light-emitting diodes, photocatalysts, as well as various photodetectors.<sup>1–4</sup> 3D hybrid halide inorganic perovskites are ionic semiconductors typically composed of lead (Pb<sup>2+</sup>), halogen anions (X<sup>-</sup> = I<sup>-</sup>, Br<sup>-</sup>, Cl<sup>-</sup>), and small organic cations or cesium (Cs<sup>+</sup>). In 2009, MAPbI<sub>3</sub> (MA = CH<sub>3</sub>NH<sub>3</sub><sup>+</sup>, methylammonium) and MAPbBr<sub>3</sub> were the first perovskites successfully applied as photovoltaic materials in a solar cell.<sup>5</sup> MAPbI<sub>3</sub> exhibits remarkable properties for solar cell applications, such as a sharp optical absorption with a large absorption coefficient of 10<sup>4</sup> cm<sup>-1</sup> and a bandgap of 1.5–1.6 eV, as evaluated by UV photoelectron or optical spectroscopy.<sup>6</sup> Moreover, MAPbI<sub>3</sub> single crystals present ultra-low trap densities, namely,

10<sup>9</sup>–10<sup>10</sup> traps per cm<sup>3</sup>, and sizable charge carrier diffusion lengths ranging within 3–10 μm.<sup>7,8</sup>

The structural, thermodynamic, and electronic properties of Pb-based halide perovskites can be tuned by substituting MA with other cations, such as Cs<sup>+</sup>, K<sup>+</sup>, and FA [FA = HC(NH<sub>2</sub>)<sub>2</sub><sup>+</sup>, formamidinium], and/or their mixtures. For example, by replacing MA with a suitable mixture of FA and Cs<sup>+</sup>, the materials' stability increases and the bandgap decreases by 0.07 eV.<sup>9</sup> Mixing halogen atoms to form mixed-halide perovskites is another efficient way of tuning the bandgap and spanning the absorption and emission energies over the UV–visible to near IR regions. Therefore, 3D halide perovskites with finely tuned Pb-based alloys of both cations and halogens are ideal for high performance solar cells, including tandems on silicon. To date, the highest certified Power Conversion Efficiency (PCE) of a Pb-based perovskite solar cell is 25.8%. This recent record was achieved, thanks to the insertion of a Cl-based coherent interlayer between the FAPbI<sub>3</sub> and the SnO<sub>2</sub> electrode.<sup>10</sup>

Despite the remarkable performance of Pb-based halide perovskites, the materials' stability under ambient conditions and the environmental concerns raised over the presence of Pb remain active challenges toward their large-scale application and commercialization.<sup>11–15</sup> Various strategies are developed to overcome these hindrances. By device or module encapsulation, the halide perovskite materials can be indeed nicely protected from exposure to moisture, UV light, heating, or air, thus mitigating the fast degradation for their long-lasting purpose.<sup>16,17</sup> On the other hand, Pb-free perovskites as well as materials derived from the perovskite structure (also called perovskite-like structures or perovskitoids), as introduced in Sec. II, are explored with the aim to obtain similar or even better properties than standard Pb-based materials.<sup>18</sup> In this Perspective, we discuss how Pb-free perovskites or perovskite-like semiconductors are used for specific optoelectronic devices, namely, solar cells, light-emitting diodes, and photocatalysts. Other explored applications include memristors, transistors, lasers, photodetectors, and various sensors.<sup>19</sup> Section II presents a classification of Pb-free materials, then we list and compare, for the best suited applications, the record performances reported so far for each class.

## II. TYPES OF LEAD-FREE PEROVSKITES

The cubic  $ABX_3$  perovskite structure within the  $Pm\bar{3}m$  space group is the reference perovskite structure. It consists of a network of corner-sharing  $BX_6$  octahedra, with the A-site atom sitting in the cuboctahedral cavity formed in between the octahedra, as shown in Fig. 1. For typical halide perovskites, a monovalent organic or inorganic cation occupies the A-site, a divalent (2+) metal, most notably Pb, is at the B-site, and the halogen anion is at the X-site. Within the lattice, A-site atoms typically only have indirect effects on the electronic structure of the materials, as the electronic states of the typical A-site cations (i.e., Cs, MA, and FA) are far from the band edges. Yet, these atoms can induce structural modifications, which in turn can lead to modifications of their electronic structure and the exhibited bandgaps. Akkerman and Manna<sup>20</sup> have recently categorized different structure types of materials based on the three- and two-dimensional (3D and 2D) ordered structures, as derived from the reference  $ABX_3$  lattice. Here, we summarize materials that are substitutionally engineered at the B-site so that all Pb atoms are replaced, only including those that have been applied in optoelectronic devices to date.

First, as  $Sn^{2+}$  and  $Ge^{2+}$  share the same nominal oxidation state with Pb, Sn- and Ge-based perovskite materials can attain the same  $ABX_3$  stoichiometry. The formed conventional  $A(Sn,Ge)X_3$  perovskite structures can adopt either the cubic reference lattice, like their Pb-based counterparts, or slightly distorted ones due to the constituents' incorporation. Moreover, since Sn, Ge, and Pb belong to the same column of the Periodic Table, they share the same electronic configuration (valency); thus, Sn and Ge-based perovskites are most likely to exhibit similar electronic and optical properties as their Pb-based counterparts. In fact, the remarkable physical and optoelectronic properties of  $APbX_3$  perovskites are known to directly relate to the antibonding electronic states:  $Pb[6s]-X[np]$  and  $Pb[6p]-X[np]$  (with  $n = 3, 4,$  and  $5$  for  $X = Cl, Br,$  and  $I$ ) located at the valence band maximum (VBM) and conduction band minimum (CBM), respectively.<sup>21</sup>

A set of popular examples of Sn-based perovskites are  $CsSnI_3$ ,  $MASnI_3$ , and  $FASnI_3$ , all of which have direct optical bandgaps in the range of 1.3–1.4 eV.<sup>18–20</sup> The electronic structure of these materials shows that the band-dispersion is similar to the Pb-based compounds, while their bandgaps are ideally placed for photovoltaic devices in the near-infrared range.<sup>22,23</sup> Yet, a well-known drawback of Sn-based perovskites is the favored oxidation of  $Sn^{2+}$  to  $Sn^{4+}$ , leading to a natural *p*-doping in samples but also to an irreversible degradation of the device performances over a short period.<sup>24,25</sup> In addition, the ease of formation of Sn vacancies results in an electrical behavior close to a metal that is far from ideal for the reproducibility, stability, and performance of devices. Therefore, the incorporation of excess  $Sn^{2+}$  in the compounds and the use of large cations are recommended in order to suppress the unwanted defects- or traps-induced recombination.<sup>26,27</sup> We note that extra care should be taken when large cations are introduced, usually to avoid disrupting the pristine crystal structure, as the materials can then form one-dimensional networks of octahedra, like in the case of  $(CH_3)_3SSnI_3$ .<sup>28</sup> Another class of materials with enhanced stability is obtained by adding large ethylenediammonium (en) cations within the  $ASnI_3$  perovskite lattice ( $A = MA, FA$ ) to form the well-known hollow perovskite lattices.<sup>29</sup>

Second, classic Ge-based perovskites are  $CsGeI_3$ ,  $MAGeI_3$ , and  $FAGeI_3$ , exhibiting direct bandgaps of 1.6, 1.9, and 2.2 eV, respectively.<sup>30</sup> Similar to the Sn-based perovskites, Ge-based ones also face stability issues due to the oxidation of  $Ge^{2+}$  to  $Ge^{4+}$ . In addition, the octahedra in  $Ge^{2+}$  based perovskites are typically heavily distorted due to the stereochemical expression of the Ge lone pair.<sup>30</sup>

Another approach toward stable and performant materials is alloying. Such an alloying strategy has been first explored for the case of mixing Pb with Sn.<sup>31</sup> These Pb/Sn mixed alloys have a smaller bandgap compared to the pristine compounds. Recently, this strategy has been expanded to fully Pb-free materials by alloying Ge with Sn, which were found to exhibit higher stabilities and narrower bandgaps than the pristine Sn and Ge-based materials, with  $CsSn_{0.5}Ge_{0.5}I_3$ , for example, exhibiting an optical bandgap of 1.5 eV.<sup>32</sup> Similar to the case of Pb-based materials, the design of 2D/3D heterostructures is another promising recipe for achieving highly efficient and stable Sn-based solar cells. Specifically, forming well-aligned 2D layers over the 3D crystal phase can considerably improve the hysteresis and light soaking of the compounds. As a consequence, the charge carrier collection, device stability, and efficiency improve with respect to the pristine 3D material.<sup>33,34</sup> Yet, the device performance of Sn and Ge based perovskites is still far from those of the Pb based counterparts, and this brings forward the indispensability of more endeavors.

Another class of materials that have been derived from the  $ABX_3$  perovskite lattice is the so-called "halide double perovskites." Many compounds have been reported since the early 1970s, often referred to as elpasolites,<sup>35</sup> and exhibit large bandgaps particularly prominent for scintillating applications. Over the past few years, a series of new halide double perovskites with relatively low bandgaps have been synthesized as possible Pb-free alternatives for optoelectronics.<sup>36–42</sup> These double perovskites keep the conventional 3D perovskite structure, but every two  $B^{2+}$  site cations are substituted by two cations B and B' with formal oxidation states of +3 and +1, as shown in Fig. 1.<sup>36–38,43</sup> The double perovskite structure corresponds to a general chemical formula of

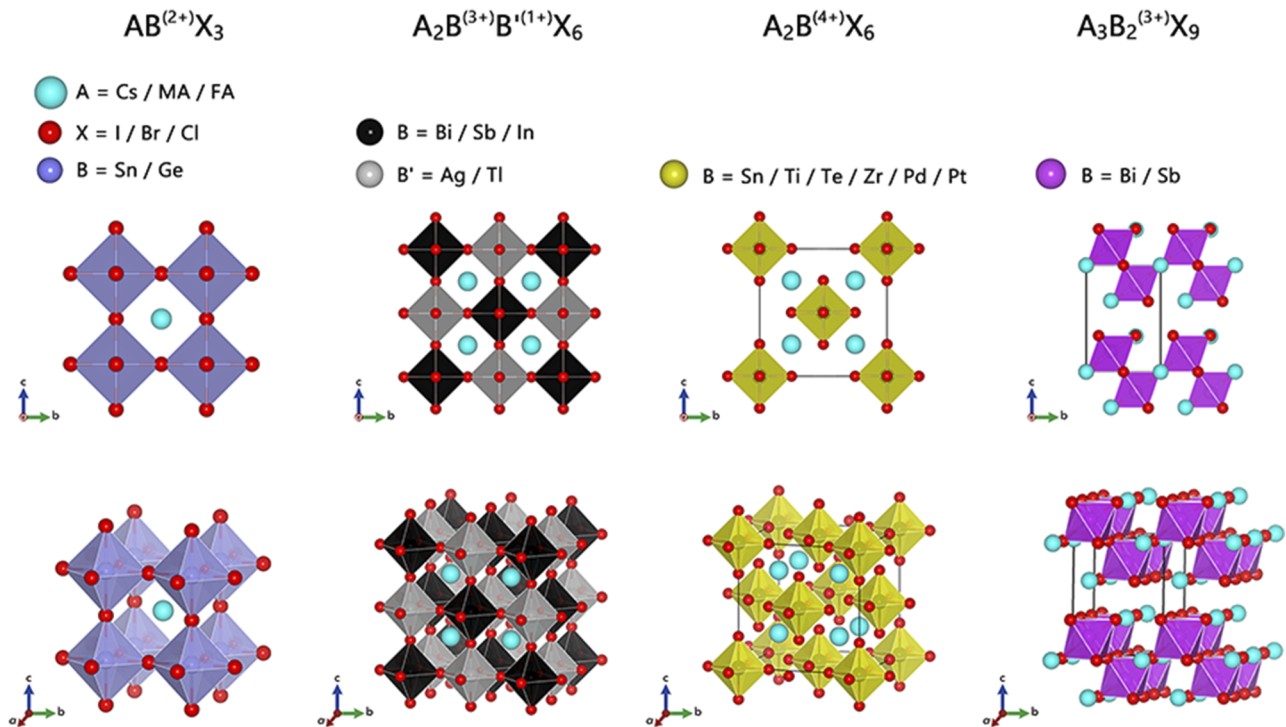


**FIG. 1.** Structure of the conventional types of Pb-free metal halide perovskites.  $AB(2+)X_3$  perovskites (with B = Sn/Ge),  $A_2B(3+)B'(1+)X_6$  double perovskites (with B = Bi/Sb/In and B' = Ag/Tl),  $A_2B(4+)X_6$  vacancy ordered double perovskites (with B = Sn/Ti/Te/Zr/Pd/Pt), and  $A_3B_2(3+)X_9$  2D layered perovskite (with B = Bi/Sb). A-site atoms can be Cs, MA, FA, and their combinations, while at the X-site, I, Br, Cl, and their combinations. Atoms A and X are in cyan and red, respectively, and atoms B or B' in four different classes are shown as octahedra.

$A_2BB'X_6$ , which is simply obtained by doubling the standard  $ABX_3$  perovskite lattice. Halide double perovskites typically crystallize in face-centered cubic  $Fm\bar{3}m$  space groups at room temperature and are known to form stable crystals under ambient conditions.<sup>37,38,44</sup> To date, the two of the most successful halide double perovskites are  $Cs_2AgBiBr_6$ <sup>37,38</sup> and  $Cs_2AgInCl_6$ ,<sup>32</sup> which have attracted much interest for optoelectronic applications as the former exhibits one of the smallest bandgaps within the halide double perovskites class (estimated at 1.95 eV<sup>36</sup>), and the latter exhibits interesting emission properties, attaining record-high photoluminescence quantum yield (PLQY) values upon appropriate doping.<sup>44</sup> Another series of low bandgap double perovskite materials that have been proposed are the ones containing  $Tl^+$  instead of  $Ag^+$ .<sup>45–47</sup> Noteworthy, besides halide perovskites, low bandgap oxide perovskites, such as  $Ba_2AgIO_6$  and  $Ba_2AuIO_6$ , which contain heptavalent iodine at the B'-site, are also explored as promising candidates for optoelectronics.<sup>48,49</sup> Another class of materials that have emerged as potentially interesting low bandgap perovskites are the so-called 111-oriented layered double perovskites.  $Cs_4CuSb_2Cl_{12}$  was first reported by Vargas *et al.*,<sup>50</sup> and there has been an increased interest in the class<sup>51</sup> and other lead-free derivatives synthesized, such as  $Cs_4CuIn_2Cl_{12}$  and  $Cs_4Cd_{1-x}Mn_xBi_2Cl_{12}$ .<sup>52,53</sup>

Starting from the  $A_2BB'X_6$  double perovskite lattice, a different class of materials can be defined by replacing the B' site with vacancies, and the B-site with a suitably charged metal to maintain

charge neutrality. These compounds are known as vacancy ordered double perovskites ( $A_2BX_6$ ), such as  $Cs_2SnI_6$  and  $Cs_2TiBr_6$ . Similar to double perovskites, the  $A_2BX_6$  lattice can be derived from the conventional perovskites by doubling the  $ABX_3$  unit cell along all three crystallographic axes but subsequently removing every other B site cation. This vacancy ordered lattice is shown in Fig. 1, and typically the materials share the same  $Fm\bar{3}m$  space group as double perovskites. Interestingly, by exposing the single  $ABX_3$  perovskite  $CsSnI_3$  to air, it can transform to the vacancy ordered  $Cs_2SnI_6$  state by the oxidation of  $Sn^{2+}$  to  $Sn^{4+}$ .<sup>54</sup> Compared to the conventional  $ABX_3$ ,  $A_2BX_6$  compounds typically possess longer B–X bonds, lower defect density, and better stability under ambient conditions. Despite being made by structurally isolated  $BX_6$  octahedra, therefore, exhibiting low structural and electronic dimensionality, some of the materials have surprisingly dispersive electronic bands and low electronic bandgaps. For example,  $Cs_2SnI_6$  has an optical bandgap of just about 1.3 eV,<sup>55,56</sup> very close to cubic  $CsSnI_3$ , and a dispersive conduction band.<sup>57</sup> Moreover, vacancy ordered halide double perovskites with Pt, Pd, Te, Ti, and Zr as the trivalent atom in the center of the octahedron have been shown to also form stable compounds and exhibit bandgaps within the near infrared.<sup>57–62</sup>

Finally, the concept of vacancy ordering can be expanded to cover another type of Pb-free materials that contain two trivalent cations that replace three  $Pb^{2+}$  atoms. The lattice of  $A_3B_2X_9$  can

be considered as a tripled  $ABX_3$  perovskite structure that contains one vacancy to maintain charge neutrality. In the lattice, as shown in Fig. 1, the vacancies are ordered along the (111) plane, making 2D layers of  $BX_6$  octahedra that crystallize usually in a trigonal  $P\bar{3}m1$  space group. These structures have been also referred to as “2D layered perovskite derivatives” and some examples of materials are  $Cs_3Bi_2Br_9$  and  $Cs_3Sb_2Br_9$ .<sup>63,64</sup> However, within the same  $A_3B_2X_9$  stoichiometry compounds, notably  $Cs_3Bi_2I_9$ <sup>65</sup> form another perovskitoid structure, within which the octahedra are face-sharing typically attaining a hexagonal  $P6_3/mmc$  space-group at room temperature. In the following, we include all  $A_3B_2X_9$  materials that have been employed in optoelectronic applications, as in some cases, materials like  $Cs_3Sb_2I_9$  and  $Cs_3Bi_2I_9$ <sup>66,67</sup> can attain both structures. These  $A_3B_2X_9$  Pb-free halide perovskites contain a pnictogen atom as the trivalent cation at the octahedra center (i.e., Sb and Bi) and are known to exhibit excellent air stability with their bandgaps ranging between 1.9 and 2.9 eV.<sup>68,69</sup>

Overall, we have summarized the structural details of the four typical prototype lattices, as shown in Fig. 1, which have been applied to date in manufacturing Pb-free optoelectronic devices. In Secs. III–V, we will overview their device performances and characteristics and highlight the emerging trends within each type of the targeted applications: solar cells, light emitters, and photocatalysts.

### III. SOLAR CELLS

Perovskite photovoltaics is the fastest ever-growing photovoltaic technology, with great potential to open the door for low-cost and efficient solar cells. This is a direct consequence of the almost perfect electronic and optical properties of Pb-based perovskites for solar cell applications. Starting from 2009, when  $MAPbI_3$  was first used as a light-sensitizer with a PCE of 3.8%,<sup>5</sup> halide perovskite solar cells have made a major step forward in 2012 by using  $MAPbI_3$  films and achieved a PCE of around 10%.<sup>70–72</sup> Interestingly, at the same period, the 3D Pb-free perovskite  $CsSnI_3$  was successfully used as a hole-conducting layer in an efficient dye-sensitized solar cell.<sup>60</sup> To date, the highest published PCE for a Pb-based perovskite solar cell is 25.8%<sup>10</sup> (certified 25.5%) obtained from the cooperation between South Korean laboratories from the Ulsan National Institute of Science and Technology (UNIST) and the Pohang Accelerator Laboratory (PAL). Furthermore, it is demonstrated that perovskite solar cells can be efficiently combined with silicon cells in tandem architectures, approaching PCE of 30% and able to overcome the performances of both separated technologies. The current certified record of 29.8% has been achieved by Helmholtz Zentrum Berlin.<sup>73</sup>

Yet, Pb-based solar cells face major stability issues, which can be at least partly tackled by considering 2D Pb-based perovskites with optimized cell configurations and device encapsulations.<sup>74,75</sup> Similar strategies are not yet fully explored for Pb-free perovskite technologies. Moreover, additives specifically dedicated to Pb-free materials may bring interesting improvements in device stability and performance. For example,  $SnF_2$ ,<sup>26</sup>  $GeI_2$ ,<sup>76</sup> or organic compounds<sup>27,77</sup> dissolved in the precursor solution contribute to the perovskite film quality, reducing surface defects/traps, attaining better crystallinity, and most importantly, completely suppressing  $Sn^{2+}$  oxidation. However, we have to note that the most efficient Pb-free

perovskite solar cells to date are not on par with the performance of Pb containing perovskites.

Table I reports the Pb-free compounds synthesized so far for solar cell applications. Their PCE (in %), open-circuit voltages (in V), and fabrication methods are listed. Among different categories of Pb-free materials, Sn-based  $ABX_3$  type perovskites show the highest PCE. This can be understood by the fact that these Sn-based  $ABX_3$  type perovskite materials exhibit very similar properties to the Pb-based ones, as discussed in Sec. II. It was reported in 2020 for  $FASnI_3$  perovskites that partially substituting FA with ethylammonium (EA) and surface passivation with 1,2-diaminoethane (EDA) can promote the crystallinity and energy band alignments with charge transport layers.<sup>76</sup> As a result, the charge carriers show enhanced mobility and longer lifetimes, resulting in an improved PCE with respect to 9% of the pristine case, with 13.24% and 12.64% for forward and reverse scans, respectively. At the beginning of 2021, the solar cell stability was improved and a maximum efficiency of 13.4% was attained.<sup>78</sup> The currently certified record efficiency amounts today to 14.6% with negligible hysteresis.<sup>79</sup> A remarkable photostability improvement was obtained in 2022 from a synergistic chemical engineering approach, leading to over 1300 h operational stability in  $N_2$  with maximum power point (MPP) tracking.<sup>80</sup> Similarly, the highest reported PCEs of  $CsSnI_3$  and  $MASnI_3$  until now are 12.96%<sup>81</sup> and 7.78%,<sup>82</sup> respectively, although it is proven theoretically that their PCEs are limited to 32.3% by comparison to 30.5% for Pb-based solar cells.<sup>83</sup> The much lower stability of Sn-based perovskite solar cells by comparison to Pb based ones even when encapsulated, leading to the exploration of surface passivation strategies.<sup>84</sup> For example, Jøker *et al.*<sup>85</sup> found that the addition of  $SnF_2$  and  $(EDA)_2I_2$  could improve the PCE and the stability of  $FASnI_3$  and that additional 20% doping of nonpolar organic cation, guanidinium ( $GA^+$ ), could increase the PCE from 7.1% to 8.5%. Furthermore, when the material ages after storage in a glove-box environment for 2000 h, the PCE of the same device tends to be 10%. Devices made of the hybrid perovskite  $(GA, FA)SnI_3$  remain stable for 1 h under continuous 1-sun illumination and for 6 days in the dark and in air without encapsulation. Very recently, dipropylammonium iodide (DipI) together with the reducing agent sodium borohydride ( $NaBH_4$ ) was shown to prevent the premature degradation of the Sn-based devices. Efficiencies above 10% were achieved with enhanced stability with 5 h in air [60% relative humidity (RH)] at MPP and 96% of the initial PCE after 1300 h at MPP in the  $N_2$  atmosphere.<sup>80</sup> According to the reported device I–V characteristics, the highest  $V_{OC}$  of Sn based perovskite solar cells reported so far is 0.96 V,<sup>79</sup> which is still significantly lower than the expected ideal value,<sup>83</sup> while the highest  $V_{OC}$  of Pb based perovskite solar cells is closer to the physical limit being over 1.3 V.<sup>86</sup>

Ge-based perovskite solar cells have achieved lower efficiencies than Sn-based ones (see Table I).  $Ge^{2+}$  oxidation under ambient air conditions causes structure instability, which is similar to the outcome of the  $Sn^{2+}$  oxidation in Sn-based perovskites. As an alternative, perovskite solar cells using alloys of Ge and Sn are developed, showing promising PCEs and better stabilities than their pure Ge equivalents due to the native-oxide passivation of surfaces. The energy band structure behavior of Sn/Ge perovskite compounds is completely different from the Sn/Pb alloys that show bandgap bowing.<sup>158</sup> Indeed, their bandgaps ( $R3m$  space group) are linearly

**TABLE I.** Solar cell applications of different Pb-free halide perovskites and their power conversion efficiencies (PCE, in %), open-circuit voltages ( $V_{OC}$ , in V), and fabrication methods. Boldface denotes state of the art results.

Category	Compounds	PCE (%)	$V_{OC}$ (V)	Fabrication method	Reference
		7.78	0.66	Spin-coating	82
		7.13	0.486	Two-step thin film deposition method	87
		6.4	0.88	Spin-coating	25
		5.44	0.716	Spin-coating	88
	MASnI <sub>3</sub>	5.23	0.68	Spin-coating	24
		3.89	0.38	Spin-coating with SnF <sub>2</sub> additive and hydrazine vapor treatment	89
		3.15	0.46	Spin-coating with SnF <sub>2</sub> additive	90
		2.14	0.45	Spin-coating with solvent bathing	91
		1.94	0.25	Spin-coating with SnF <sub>2</sub> additive	92
		1.86	0.273	Low-temperature vapor assisted solution deposition process	93
		1.7	0.38	Thermal co-evaporation	93
	MASnI <sub>2</sub> Br	5.48	0.77	Spin-coating	24
	MASnI <sub>2</sub> Br <sub>2</sub>	5.73	0.82	Spin-coating	24
	MASnBr <sub>3</sub>	4.27	0.88	Spin-coating	24
		1.12	0.498	Vapor deposition	94
	MASnBr <sub>0.5</sub> I <sub>2.5</sub>	1.05	0.18	Spin-coating	95
	MASnI <sub>1.8</sub> Cl <sub>0.2</sub>	3.1	0.38	Drop casting	96
	MA <sub>0.9</sub> CS <sub>0.1</sub> SnI <sub>3</sub>	0.51	0.49	Vapor assisted solution deposition process	97
		0.3	0.20	Spin-coating	98
	(FA <sub>0.9</sub> EA <sub>0.1</sub> ) <sub>0.98</sub> EDA <sub>0.02</sub> SnI <sub>3</sub>	13.2	0.84	Spin-coating with GeI <sub>2</sub> additive	76
	FA <sub>0.98</sub> EDA <sub>0.01</sub> SnI <sub>3</sub>	12.2	0.70	92 days of storage in N <sub>2</sub> : 80% PCE	99
	PEA <sub>0.15</sub> FA <sub>0.85</sub> SnI <sub>3</sub> + NH <sub>4</sub> SCN	12.4	0.94	Spin-coating with SnF <sub>2</sub> additive	100
	FA <sub>0.9</sub> EA <sub>0.1</sub> SnI <sub>3</sub>	11.75	0.65	Spin-coating with GeI <sub>2</sub> additive	76
	PEA <sub>0.15</sub> FA <sub>0.85</sub> SnI <sub>3</sub>	7.1	0.78	Spin-coating with SnF <sub>2</sub> additive	100
	FASnI <sub>3</sub> + 4-(aminomethyl) piperidinium	10.9	0.69	Spin coating	101
	FASnI <sub>3</sub>	10.1	0.63	Spin coating with FAI, SnI <sub>2</sub> , and SnF <sub>2</sub> additive	102
		13.4	0.81	Spin-coating with phenylhydrazine	78
		<b>14.6<sup>a</sup></b>	0.96	Spin-coating with adducts	79
		10.6	0.66	<b>Stability record<sup>a</sup></b>	80
	FASnI <sub>3</sub>	9.03	0.72	Spin-coating with GeI <sub>2</sub> additive	76
		6.75	0.58	Spin-coating with Sn powder additive	103
		6.6	0.48	Spin-coating with SnF <sub>2</sub> additive	104
		6.48	0.553	Spin-coating with SnF <sub>2</sub> additive	105
		6.22	0.48	Spin-coating with SnF <sub>2</sub> additive	106
		5.27	0.38	Spin-coating with diethyl ether dripping and SnF <sub>2</sub> additive	107
ABX <sub>3</sub>		4.8	0.32	Spin-coating with pyrazine mediator and SnF <sub>2</sub> additive	107
		3.12	0.31	Spin-coating with SnF <sub>2</sub> and HPA additive	108
		2.10	0.24	additive Spin-coating	109
		8.92	0.63	Spin-coating with SnF <sub>2</sub> additive	105
	FASnI <sub>3</sub> + 2,3-diaminopropionic acidmonohydrochloride (2,3-DAPAC)	7.23	0.52	Spin-coating with SnF <sub>2</sub> additive	110

TABLE I. (Continued.)

Category	Compounds	PCE (%)	V <sub>OC</sub> (V)	Fabrication method	Reference
	FASnI <sub>2</sub> Br	1.72	0.47	Spin-coating	109
	Br-doped FASnI <sub>3</sub>	5.5	0.41	Spin-coating with pyrazine mediator and SnF <sub>2</sub> additive	111
	FA <sub>0.8</sub> MA <sub>0.2</sub> SnI <sub>3</sub>	1.4	0.24	Spin-coating solvent engineering	98
	FA <sub>0.25</sub> MA <sub>0.75</sub> SnI <sub>3</sub>	4.49	0.48	Spin-coating with SnF <sub>2</sub> additive	104
	FA <sub>0.5</sub> MA <sub>0.5</sub> SnI <sub>3</sub>	5.92	0.53	Spin-coating with SnF <sub>2</sub> additive	104
	FA <sub>0.75</sub> MA <sub>0.25</sub> SnI <sub>3</sub>	8.12	0.61	Spin-coating with SnF <sub>2</sub> additive and chlorobenzene dripping	104
		9.06	0.55	Spin-coating + SnF <sub>2</sub> additive and chlorobenzene dripping + post-annealing	112
	FA <sub>0.75</sub> MA <sub>0.25</sub> SnI <sub>3</sub> CsSnI <sub>3</sub> + phthalimide (PTM)	7.2	0.55	Spin-coating with SnF <sub>2</sub> additive and hot antisolvent treatment and solvent vapor annealing	113
		3.31	0.46	Spin-coating + antisolvent	114
		2.60	0.37	Spin-coating + SnF <sub>2</sub> additive	115
		10.1	0.64	Two-step spin-coating + chlorobenzene as antisolvent	77
	CsSnI <sub>3</sub> + thiosemicarbazide (TSC)	8.20	0.63	Passivator assisting sequential vapor deposition	84
	CsSnI <sub>3</sub>	4.81	0.38	Spin-coating with SnI <sub>2</sub> additive	116
		3.83	...	Spin-coating with SnF <sub>2</sub> and piperazine additive	117
		3.56	0.50	Spin-coating with SnCl <sub>2</sub> additive	118
		3.31	0.52	Spin-coating and annealing	119
		2.76	0.43	Spin-coating with SnI <sub>2</sub> additive	120
	CsSnI <sub>3</sub>	2.02	0.24	Spin-coating with SnF <sub>2</sub> additive	121
	FA <sub>0.75</sub> MA <sub>0.25</sub> Sn <sub>0.95</sub> Ge <sub>0.05</sub> I <sub>3</sub>	1.83	0.17	Spin-coating with SnF <sub>2</sub> additive and hydrazine vapor treatment	89
		1.70	...	Solid-state reaction	32
		1.66	0.20	Spin-coating with SnF <sub>2</sub> additive	81
		0.90	0.42	Sequential evaporation and subsequent annealing	121
		7.90	0.45	Spin-coating + GeI <sub>2</sub> and SnF <sub>2</sub> additives	115
	FA <sub>0.75</sub> MA <sub>0.25</sub> Sn <sub>0.95</sub> Ge <sub>0.05</sub> I <sub>3</sub> Native oxide passivated	4.48	0.42	Spin-coating + antisolvent	114
		7.11	0.63	Solid-state reaction	32
	CsSn <sub>0.5</sub> Ge <sub>0.5</sub> I <sub>3</sub>	3.72	0.48	Solid-state reaction + N <sub>2</sub>	32
	CsSn <sub>0.5</sub> Ge <sub>0.5</sub> I <sub>3</sub>	1.76	0.22	Spin-coating with SnF <sub>2</sub> additive	122
	CsSnI <sub>2.9</sub> Br <sub>0.1</sub>	1.67	0.29	Spin-coating with SnF <sub>2</sub> additive	81
	CsSnI <sub>2</sub> Br	3.20	0.31	Sequential evaporation and subsequent annealing	122
	CsSnI <sub>2</sub> Br	1.56	0.31	Sequential evaporation and subsequent annealing	81
	CsSnBr <sub>3</sub>	3.04	0.37	Spin-coating with SnF <sub>2</sub> additive and hydrazine vapor treatment	89
		2.10	0.41	Spin-coating with SnF <sub>2</sub> additive	123
	CsSnBr <sub>3</sub>	0.95	0.41	Spin-coating with SnF <sub>2</sub> additive	81
	CsSnI <sub>3</sub> (QR)	0.55	0.45	All vapor deposited with SnF <sub>2</sub> additive	124
		13.0	0.86	Spin-coating	81
	CsSnBr <sub>3</sub> (QR)	10.5	0.85	Spin-coating	81
	CsSnCl <sub>3</sub> (QR)	9.66	0.87	Spin-coating	118

TABLE I. (Continued.)

Category	Compounds	PCE (%)	V <sub>OC</sub> (V)	Fabrication method	Reference
	MAGeI <sub>3</sub>	0.68	...	...	125
	MAGeI <sub>3</sub>	0.20	0.150	...	125
	MAGeI <sub>2.7</sub> Br <sub>0.3</sub>	0.57	0.449	Spin-coating	125
	CsGeX <sub>3</sub>	4.94	0.51	Quantum rods	126
	CsGeI <sub>3</sub>	0.11	0.074	...	127
	{en}MASnI <sub>3</sub>	6.63	0.43	Spin-coating with SnF <sub>2</sub> additive	128
	{en}FASnI <sub>3</sub>	7.14	0.48	Spin-coating with SnF <sub>2</sub> additive	29
	{en}FA <sub>0.78</sub> GA <sub>0.22</sub> SnI <sub>3</sub>	9.60	0.619	Spin-coating with SnF <sub>2</sub> additive	85
	Cs <sub>2</sub> AgBiBr <sub>6</sub> + carboxy-chlorophyll derivative (C-chl)	<b>3.11<sup>a</sup></b>	1.04	Spin-coating	129
	Cs <sub>2</sub> AgBiBr <sub>6</sub>	2.84	1.06	Spin-coating	130
	Cs <sub>2</sub> AgBiBr <sub>6</sub>	2.43	0.98	Spin-coating	131
A <sub>2</sub> BB'X <sub>6</sub>	(Cs <sub>0.9</sub> Rb <sub>0.1</sub> ) <sub>2</sub> AgBiBr <sub>6</sub>	2.23	1.01	Spin-coating with antisolvent	132
		1.44	1.04	Spin-coating	132
		1.26	1.02	Spin-coating with antisolvent	131
		1.37	1.12	Sequential vapor deposition	133
	Cs <sub>2</sub> NaBiI <sub>6</sub>	1.52	0.99	Spin-coating	134
	Cs <sub>2</sub> NaBiI <sub>6</sub>	0.42	0.47	One-step hydrothermal process	135
	Cs <sub>2</sub> SnI <sub>6</sub>	0.96	0.51	Thermal evaporation, annealing, and phase change	136
	Cs <sub>2</sub> SnI <sub>6</sub>	0.86	0.52	Spin-coating	137
	Cs <sub>2</sub> SnI <sub>5</sub> Br	1.47	0.37	Two-step thin film deposition method	138
		0.47	0.25	Chemical bath deposition	139
	Cs <sub>2</sub> SnI <sub>4</sub> Br <sub>2</sub>	1.60	0.44	Two-step thin film deposition method	138
A <sub>2</sub> BX <sub>6</sub>	Cs <sub>2</sub> SnI <sub>4</sub> Br <sub>2</sub>	2.03	0.56	Two-step thin film deposition method	138
	Cs <sub>2</sub> SnI <sub>2</sub> Br <sub>4</sub>	1.08	0.58	Two-step thin film deposition method	138
	Cs <sub>2</sub> SnIBr <sub>5</sub>	0.002	0.57	Two-step thin film deposition method	138
	Cs <sub>2</sub> TiBr <sub>6</sub>	3.28	1.02	Two-step vapor deposition	140
	Cs <sub>2</sub> TiBr <sub>6</sub>	2.26	0.89	Two-step vapor deposition	140
	Cs <sub>2</sub> SnI <sub>3</sub> Br <sub>3</sub>	<b>3.63<sup>a</sup></b>	0.70	Two-step thin film deposition method with Z907 dye	141
		1.64	0.81	Deposition and homogeneous transformation	63
		0.42	0.67	Deposition and homogeneous transformation	142
		0.39	0.81	Thermal evaporation, spin-coating, and annealing	143
		0.36	0.65	Solvent engineering	144
	MA <sub>3</sub> Bi <sub>2</sub> I <sub>9</sub>	0.31	0.51	Spin coating	145
	MA <sub>3</sub> Bi <sub>2</sub> I <sub>9</sub>	0.26	0.56	Spin-coating	63
	MA <sub>3</sub> Bi <sub>2</sub> I <sub>9</sub> Cl <sub>x</sub>	0.19	0.35	Spin-coating	146
		0.12	0.68	Spin-coating	146
		0.11	0.72	Solvent engineering	147
		0.08	0.69	Spin coating with gas-assisted	148
		0.07	0.66	Spin coating	149
		0.053	0.84	Spin-coating	150
	MA <sub>3</sub> Sb <sub>2</sub> I <sub>9</sub>	0.003	0.04	Spin-coating	146
		2.77	0.70	Spin-coating with pyrene/HI + chlorobenzene additive	151
	MA <sub>3</sub> Sb <sub>2</sub> I <sub>9</sub>	2.46	0.69	Spin-coating with perylene/HI + chlorobenzene additive	151
A <sub>3</sub> B <sub>2</sub> X <sub>9</sub>	MA <sub>3</sub> Sb <sub>2</sub> I <sub>9</sub>	2.25	0.63	Spin-coating with HI + chlorobenzene additive	151
	MA <sub>3</sub> (Sb <sub>0.6</sub> Sn <sub>0.4</sub> ) <sub>2</sub> I <sub>9</sub>	1.89	0.62	Spin-coating with HI additive	151
		2.04	0.62	Spin-coating with HI additive	152
		0.62	0.75	Spin-coating with chlorobenzene dripping	153
		0.5	0.89	Spin-coating	154
	CsBi <sub>3</sub> I <sub>10</sub>	<b>2.80<sup>a</sup></b>	0.57	Spin-coating with chlorobenzene dripping	153

TABLE I. (Continued.)

Category	Compounds	PCE (%)	V <sub>OC</sub> (V)	Fabrication method	Reference
	CsBi <sub>3</sub> I <sub>10</sub>	<b>0.40</b>	0.31	Spin-coating	155
	Cs <sub>3</sub> Bi <sub>2</sub> I <sub>9</sub>	1.09	0.85	Spin-coating	146
	Cs <sub>3</sub> Bi <sub>2</sub> I <sub>9</sub>	0.02	0.26	Spin-coating	155
	Cs <sub>3</sub> Sb <sub>2</sub> I <sub>9</sub>	0.84	0.60	Spin-coating with HI additive	152
	Rb <sub>3</sub> Sb <sub>2</sub> I <sub>9</sub>				
	Cs <sub>3</sub> Sb <sub>2</sub> I <sub>9</sub>	<1	0.30	Dual annealing	152
	Rb <sub>3</sub> Sb <sub>2</sub> I <sub>9</sub>				
	(NH <sub>4</sub> ) <sub>3</sub> Sb <sub>2</sub> I <sub>9</sub>	0.66	0.55	Spin-coating with toluene dripping	156
	(NH <sub>4</sub> ) <sub>3</sub> Sb <sub>2</sub> I <sub>9</sub>	0.51	1.03	Spin-coating with chloroform dripping	157

<sup>a</sup>The highest value of PCE for each category of Pb-free perovskites, as highlighted in a bold font.

increasing with respect to the concentration of Ge.<sup>159</sup> For instance, the CsSn<sub>0.5</sub>Ge<sub>0.5</sub>I<sub>3</sub> has a bandgap (1.50 eV) in between CsSnI<sub>3</sub> (1.31 eV) and CsGeI<sub>3</sub> (1.63 eV) and allows photo-absorption across the visible light region.<sup>32</sup> As a result, a PCE of 7.11% is obtained for CsSn<sub>0.5</sub>Ge<sub>0.5</sub>I<sub>3</sub> in comparison to the 3.72% attained without forming a native-oxide layer and the 1.7% of the pure CsSnI<sub>3</sub>. As discussed previously, mixing halides might lead to chemical inhomogeneities in the conventional perovskite compounds. However, mixed-halide CsSn<sub>1-x</sub>Ge<sub>x</sub>I<sub>3-y</sub>Br<sub>y</sub> compounds are easier to synthesize than the single-halide CsSn<sub>1-x</sub>Ge<sub>x</sub>I<sub>3</sub> compounds and are superior in terms of optical response in the visible light range, according to Chang *et al.*<sup>160</sup> Among them, the CsSn<sub>0.5</sub>Ge<sub>0.5</sub>I<sub>2</sub>Br is the best choice. To date, the highest PCE of Sn/Ge alloys amounts to 7.9%, with FA<sub>0.75</sub>MA<sub>0.25</sub>Sn<sub>0.95</sub>Ge<sub>0.05</sub>I<sub>3</sub> based solar cells fabricated by passivating and reducing trap densities with GeI<sub>2</sub> and SnF<sub>2</sub> additives.<sup>115</sup> More importantly, the PCE retains 91% of its initial value for 500 h under 1-sun illumination in air. Although the results of Sn/Ge mixed perovskites are encouraging, they are still far from the expected maximum PCE value. For instance, the theoretical predicted PCE of CsSn<sub>0.5</sub>Ge<sub>0.5</sub>I<sub>3</sub> is as high as 24.20%.<sup>161</sup>

Double perovskites and vacancy ordered double perovskites are very stable under ambient conditions. Yet, the electronic bandgaps of the synthesized double perovskites range from 2 to 3.4 eV and thus are too large for efficient light harvesting in single-junction photovoltaics. The highest PCE obtained for a double perovskite, 3.11% obtained for Cs<sub>2</sub>AgBiBr<sub>6</sub>, is, nevertheless, a decent achievement for a large bandgap semiconductor.<sup>129</sup> Doping with In, a common strategy for highly efficient light emitters discussed below, could also improve the attained photovoltaic performance as recently shown by Schade *et al.*<sup>162</sup> More generally, their stability combined with their optoelectronic properties, including photoconversion at high energy, light emission, and charge transport, might be more attractive for other optoelectronic applications.

Meanwhile, the highest PCE obtained for a vacancy ordered double perovskite is 3.63% for the mixed-halide Cs<sub>2</sub>SnI<sub>3</sub>Br<sub>3</sub>.<sup>141</sup> Since the Sn atoms used in vacancy ordered double perovskites correspond to the +4 oxidation state, these perovskite structures are the most stable among Sn based perovskite materials under ambient conditions.

Although Pb-free A<sub>3</sub>B<sub>2</sub>X<sub>9</sub> 2D perovskite derivatives are quite stable in air, their achieved PCE remained much lower than 1% without improvement for a long time. A breakthrough was obtained in 2018 for Pb-free 2D perovskite based on Sb dimers with the help of additives and antisolvents treatment. A continuum, smooth, and pinhole-free morphology of MA<sub>3</sub>Sb<sub>2</sub>I<sub>9</sub> can be formed, thanks to fast heterogeneous nucleation, yielding a record PCE of 2.77%.<sup>151</sup> In the same year, a PCE of 2.80% was achieved for MA<sub>3</sub>(Sb<sub>1-x</sub>Sn<sub>x</sub>)<sub>2</sub>I<sub>9</sub> by heterovalent substitution when x is 0.4, contrasting to a PCE of 0.62% when x is 0.<sup>153</sup> By Sn<sup>4+</sup> substitution, the bandgap is reduced from the pristine bandgap value of 2 eV close to the optimum value of 1.55 eV, and the electronic conductivity is changed from p-type to n-type, leading to a better band alignment with the selected contact layers. All the above discussions point out that chemical engineering, additives, antisolvent treatment, and hydrophobic charge transport layers are the guides to further improve the PCEs of double and 2D Pb-free perovskites.

To establish a connection between the types of Pb-free materials and their application in solar cells, we calculate the percentage of each type of Pb-free materials that have been reported in solar cell applications. Figure 2(a) highlights the contribution of the conventional single ABX<sub>3</sub> (pink color), double A<sub>2</sub>BB'X<sub>6</sub> (cyan color), vacancy ordered double A<sub>2</sub>BX<sub>6</sub> (gray color), and 2D layered A<sub>3</sub>B<sub>2</sub>X<sub>9</sub> Pb-free perovskites (orange color) by the inner ring of the sunburst chart, where their percentages are listed at the inner blank spaces, which are 62%, 7%, 9%, and 22%, respectively. In addition, the contributions of different types of B site cations are highlighted by the outer ring of the sunburst chart, where the corresponding percentages are summarized at the outer blank spaces. In addition, the contribution of A site cations and X site anions is represented by the 3D pie charts, where their corresponding percentages are summarized next to each of them.

Among all Pb-free compounds, most materials contain Sn, with 90% of the cubic perovskites and 82% of the vacancy ordered double perovskites being Sn-based compounds. This is in line with the favorable PCEs of Sn based perovskite solar cells being the most promising to date. Among all Sn-based compounds used for solar cell applications, 89% of Sn compounds are materials with Sn in the +2 oxidation state, which is consistent with the fact that stability

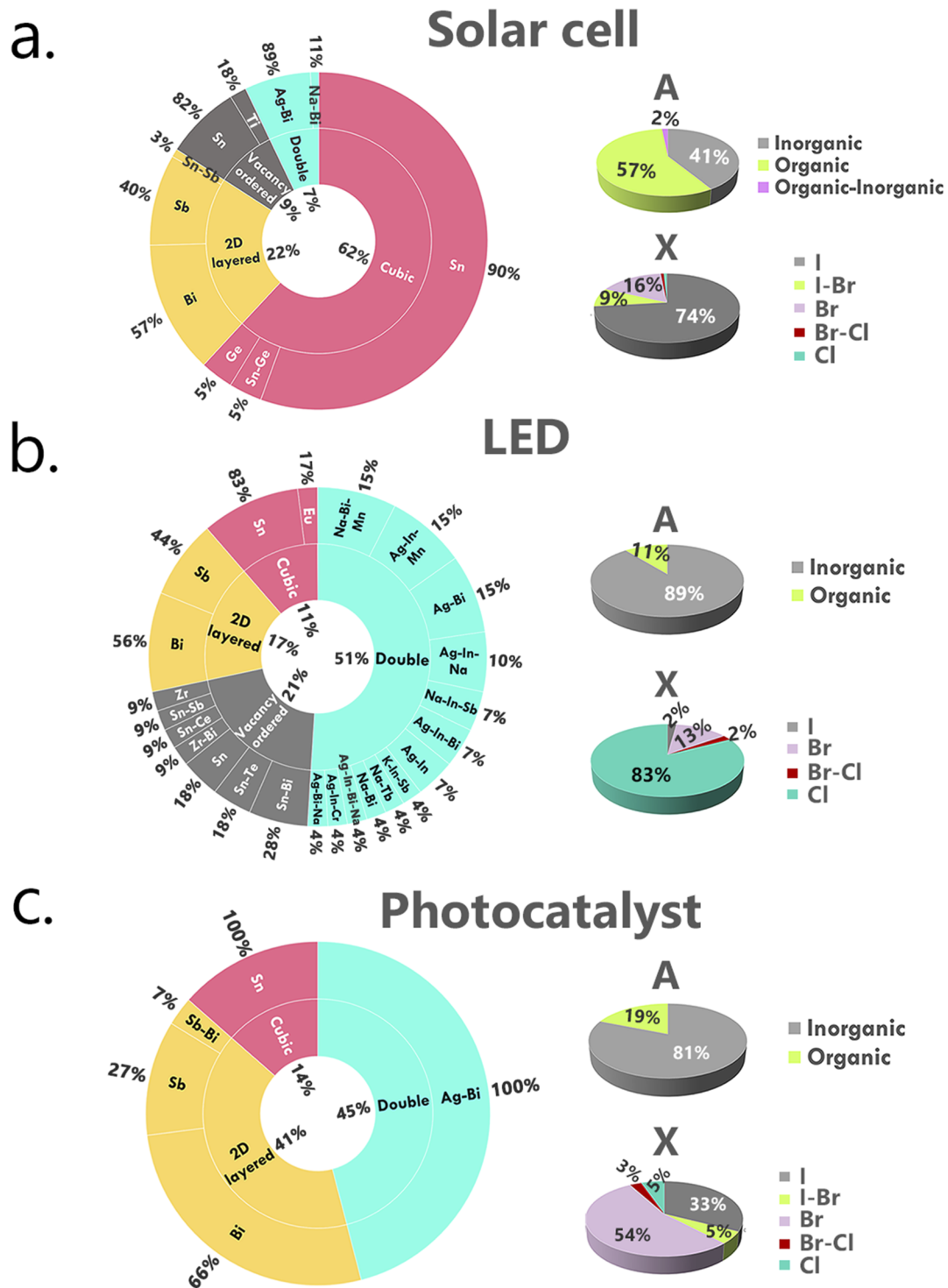


**FIG. 2.** Sunburst charts showing the use of different Pb-free halide perovskite classes (conventional  $ABX_3$  in pink, double  $A_2BB'X_6$  in cyan, vacancy ordered double  $A_2BX_6$  in gray, and 2D layered  $A_3B_2X_9$  in orange) in the fabrication of solar cells (top), LEDs (middle), and photocatalysts (bottom). In each chart, the contribution of different perovskite classes is highlighted by the inner ring, and their percentages are summarized at the inner blank spaces; the contribution of different B site cations in each class is highlighted by the outer ring with the same color as the inner ring, and their percentages are summarized at the outer blank spaces. The corresponding distribution in terms of different A site cations and X site anions is shown in the 3D pie charts (right panels). Percentages below 1% are not included.

remains the main issue in this field. Therefore, the still rare (5%) use of either pure Ge (5%) or mixtures of Ge and Sn might become the next step in the quest for stable Pb-free perovskite solar cell applications. Among  $A_2BB'X_6$  double perovskites, the ones based on  $B = \text{Bi}$  and  $B' = \text{Ag}$  (including doped derivatives) are almost the sole Pb-free candidates to date that have been tested for solar cells; those based on  $B = \text{Bi}$  and  $B' = \text{Na}$  have merely achieved a PCE of 0.4%. In addition, in 2D layered perovskites, most of the B site cations are either Bi (57%) or Sb (40%), with a small percentage (3%) of Bi–Sb mixtures. In addition, from the 3D pie chart indicative of the halide species, as for Pb-based perovskites, most compositions used for solar cell applications are iodides (74%), followed by bromides (16%) and mixed I–Br compounds (9%). In contrast, the Cl and mixed Br–Cl compounds are rarely used (less than 1%). Finally, organic (57%) and inorganic (41%) A-site cations are almost equally used, with a small amount (2%) of organic–inorganic mixtures.

#### IV. LIGHT EMISSION

Over the past decades, thanks to their intrinsic properties, including high PLQY, Pb-based metal halide perovskites have also gained great interest for LED applications. For example, Zhou *et al.*<sup>163</sup> achieved a record-high PLQY of 94.6% with  $\text{MAPbX}_3$  ( $X = \text{Cl}, \text{Br}, \text{I}$ ) nanocrystals embedded in polyvinylidene fluoride composite films. However, achieving large external quantum efficiencies (EQE) in operating LED devices requires more, especially good carrier transport and carrier injection from the electrical contacts toward the active zone. Once these conditions are fulfilled, it is considered nowadays that perovskite-based LEDs should overcome EQE of 20% starting from high PLQY, thanks to photon recycling and efficient optical outcoupling.<sup>164</sup> Green LEDs are the best performing devices, leading to a maximum EQE of 28.1% in 2021.<sup>165</sup> Using non-perovskite matrices was also successful for Pb-based green emitters leading to stable operation over 50 h with an EQE of 15%.<sup>166</sup> This solution has the disadvantage of putting strong practical limits on the current injected into the active zone (1.2 mA cm<sup>-2</sup> in Ref. 166) but may provide some guidance for the design of Pb-free emitters. Pb-based red LEDs emitting at 627 nm with an impressive EQE of 20.3% (starting from a PLQY of 88%) were obtained recently, although the operational stability remains limited to 1 h and the EQE drops very quickly for current densities above 1 mA cm<sup>-2</sup>. The performances of blue Pb-based LEDs are more limited leading, for example, to an EQE of 12.3% starting from a PLQY over 90%,<sup>167</sup> or a sky-blue emitting device with an EQE of 13.8% but driven by a high voltage of above 4 V.<sup>168</sup> Finally, it shall be mentioned that demonstrations of single layer Pb-based white light LED do exist,<sup>169</sup> although with room for improvement. A promising EQE of 1.2% (starting from a PLQY of 85%) with a color rendering index (CRI) of 93 was, for example, obtained in 2020 using  $\text{CsPbCl}_3$  quantum dots doped with  $\text{Sm}^{3+}$ .<sup>170</sup> It is now clear that Pb-based perovskites are nowadays strong competitors in the field of LEDs, with remarkable EQE demonstrations for monochromatic red, green, or blue optical sources and even promising single layer white-light emitters. However, challenges are still remaining for commercialization including among others, highly efficient blue electroluminescence, long device lifetime, toxicity, and bioavailability of lead.<sup>171</sup>

From the perspective of LED engineering, the quality of the interfaces is of utmost importance as mentioned above. This additional constraint might hinder the practical application of most Pb-free perovskite materials to LEDs, despite exhibiting attractive PLQY. So far, most of the experimental data reported on Pb-free materials to illustrate light emission capabilities are related to the PLQY. This interesting piece of information shall be handled with care since it might not guarantee LEDs with attractive performances. We already saw indeed in Sec. III on solar cells that interface issues are limiting the performances of Pb-free perovskite devices. It shall be further pointed out that current densities flowing through operating LED devices may exceed by one order of magnitude the current densities observed in solar cells. This may put even more stringent requirements on the Pb-free material quality and their interfaces with carrier transporting layers. In this Perspective, we, nevertheless, limit our overview of Pb-free perovskite performances to PLQYs, leaving aside EQEs mainly due to the lack of extensive data in the literature.

As it seems Pb-free materials can hardly compete with Pb-based ones for solar cells due to their low PCEs, this might be also the case for LED applications. Their high tunability across the entire visible light spectrum might be nevertheless one comparative advantage.<sup>163,172–174</sup> Narrowband emission, usually observed at low temperature, is very often attributed to intrinsic free excitonic transitions. Such transitions can be influenced by lattice parameters and thermal expansion mismatches between perovskites and charge transport layers. An additional broadband emission at low energy is also observed in some cases. This broadband emission is believed to have good potential for white light LEDs. Self-trapping excitons (STEs) are very often claimed to be at the origin of this broad red-shifted, but extrinsic or defect-related emission mechanisms are still not ruled out.

Among the four classes of Pb-free perovskites, double perovskites and vacancy ordered double perovskites show promising PLQYs as well as high intrinsic thermodynamic stabilities and low carrier effective masses. One of the major challenges is their wide and/or indirect bandgaps, which makes them less suitable for optoelectronic applications in the visible region. For this reason, homovalent and heterovalent co-doping have been developed.  $\text{Cs}_2\text{AgBiCl}_6$  and  $\text{Cs}_2\text{AgInCl}_6$  have become the reference materials for realizing white light LEDs for Pb-free materials. In comparison to pure  $\text{Cs}_2\text{AgBiCl}_6$ , the higher stability of Na-doped  $\text{Cs}_2(\text{Na}_{1-x}\text{Ag}_x)\text{BiCl}_6$  was attributed to the easier formation of a  $[\text{NaCl}_6]^{5-}$  octahedron compared to a  $[\text{AgCl}_6]^{5-}$  one, but this, in turn, results in a larger bandgap.<sup>175</sup> It is also found that the minor luminescence of the as-prepared  $\text{Cs}_2\text{NaInCl}_6$  nanocrystals (dark STEs) can convert into a bright yellow emission (attributed to bright STEs) by  $\text{Ag}^+$  doping.<sup>176</sup> Two physical mechanisms have been proposed to explain the enhanced light emissions.<sup>177</sup> First,  $[\text{NaCl}_6]^{5-}$  and  $[\text{AgCl}_6]^{5-}$  octahedra can break the parity-forbidden selection rule for the direct optical transition hence stimulating effective photoluminescence (PL) emission. Second, the presence of  $\text{Ag}^+$  can mitigate the effect of lattice vibrations on PL quenching.  $\text{Sb}^{3+}$ ,  $\text{In}^{3+}$ , and  $\text{Mn}^{2+}$  doping are also popular choices for tuning the electronic properties. For example, the Sb- and In-doping of  $\text{Cs}_2\text{AgBiBr}_6$  induce opposite variations of the bandgaps, leading to an increase (decrease) for  $\text{In}^{3+}$  ( $\text{Sb}^{3+}$ ) doping. It has to be noted that  $\text{Sb}^{3+}$  doping produces the smallest bandgap within this class, with a value of

1.86 eV for  $\text{Cs}_2\text{Ag}(\text{Bi}_{0.625}\text{Sb}_{0.375})\text{Br}_6$ . In addition, these doped systems are only stable when  $\text{In}^{3+}$  and  $\text{Sb}^{3+}$  doping ratios are within the 0%–75% and 0%–37.5% ranges, respectively.<sup>178</sup>

Substituting or doping double perovskites that contain Bi (or Sb) with In results in an interplay between direct and indirect bandgaps,<sup>32,155,179</sup> which could be promising for the luminescence of perovskite phosphors toward white-light emission. In contrast, the bandgaps of  $\text{Cs}_2\text{AgInCl}_6$  double perovskites have no significant difference before and after  $\text{Mn}^{2+}$  doping.<sup>180</sup> However, with Mn-doping as high as 1.5%, the weak PL of undoped  $\text{Cs}_2\text{NaBiCl}_6$  has been enhanced to emit a new orange-red PL (from 525 to 700 nm). The PLQY increases by an order of magnitude, namely, from 1.6% up to 16%. This enhanced emission has been attributed to the near-UV light absorption of  $[\text{BiCl}_6]^{3-}$  octahedra in the host lattice and the energy transfer from  $\text{Bi}^{3+}$  to  $\text{Mn}^{2+}$  activators via the spin-forbidden  $^4\text{T}_1 \rightarrow ^6\text{A}_1$  transition.<sup>181</sup> This  $^4\text{T}_1 \rightarrow ^6\text{A}_1$   $d-d$  transition is expected to interact less with nonradiative trap states in the host lattice, accounting for the enhanced PL intensity and millisecond long lifetime.<sup>154</sup> As reported in the literature,<sup>182</sup> the internal quantum efficiency of  $\text{Cs}_2(\text{Ag}_{0.4}\text{Na}_{0.6})\text{InCl}_6$ : 1% Bi phosphor can be further increased from 89.9% to 98.4% and 98.6% by co-doping 1% Ni and 1% Ce, respectively. The physical mechanisms at the origin of light emission depend on the nature of the perovskite host. Specifically, for Mn-doped  $\text{Cs}_2(\text{Na}_{0.75}\text{Ag}_{0.25})\text{BiCl}_6$ , the distinct energy-transfer channel from  $\text{Mn}^{2+}$  ion guest to STEs perovskite host has been proposed to result in the dominant  $\text{Mn}^{2+}$  emission,<sup>175</sup> which is similar to pure  $\text{Cs}_2\text{AgInCl}_6$ .<sup>180</sup> In contrast, for Mn-doped  $\text{Cs}_2(\text{Na}_{0.4}\text{Ag}_{0.6})\text{In}_{0.95}\text{Bi}_{0.05}\text{Cl}_6$ , the efficient energy transfer from broadband STEs host to  $\text{Mn}^{2+}$  guest  $d-d$  transitions would explain the high PLQY.<sup>183</sup> In addition to the above two mechanisms, for the Mn-doped  $(\text{C}_6\text{H}_{18}\text{N}_2\text{O}_2)\text{PbBr}_4$ , the tentative explanation for the ultrabroad band warm light emission relies on a simultaneous enhancement of STE emission and  $\text{Mn}^{2+}$  emission.<sup>184</sup>

Table II presents, for the four material classes, the Pb-free perovskite compositions synthesized to date for LED applications, together with their emission peak positions (in nm), the light emission colors, the full-width half maxima (FWHM, in nm) of the emissions, and the PLQYs (in %). We note that the highest PLQY of about 93% has been achieved with Sb-doped  $\text{Cs}_2\text{KInCl}_6$ .<sup>185</sup> Apart from double perovskites, vacancy ordered double perovskites also appear as promising candidates for LED applications. The highest PLQY among them is obtained for Te-doped  $\text{Cs}_2\text{SnCl}_6$ , with 95.4%.<sup>186</sup> Replacing  $\text{Sn}^{4+}$  with  $\text{Te}^{4+}$  is proposed to lead to the generation of new defect levels above band edges, which promote an exciton transition nearby  $[\text{TeCl}_6]^{2-}$  octahedra, thereby initiating STEs emission of broad yellow–green luminescence.<sup>186</sup> This  $\text{Te}^{3+}$  triggered STEs emission is also hypothesized in the A site organic perovskite  $(\text{NH}_4)_2\text{SnCl}_6$ , whose PLQY increases from less than 0.05% before  $\text{Te}^{3+}$  doping to 83.5% after doping.<sup>187</sup> Noteworthy, the good stability against water of the Te-doped  $\text{Cs}_2\text{SnCl}_6$  makes it particularly suitable for underwater lighting applications.<sup>186</sup>

The statistical overview of different classes and compositions of Pb-free perovskites explored to date for LED applications is also shown in Fig. 2(b). Among all Pb-free compounds synthesized for LED applications, 51% are double perovskites and 21% belong to the vacancy ordered double perovskites. The percentages of conventional perovskites and 2D layered perovskites are relatively smaller,

with 11% and 17%, respectively. Unlike in conventional perovskites where the B site is always Sn, in double perovskites, B site cations are often mixtures of two or three types of cations, such as Ag–Bi (15%), Na–Bi–Mn (15%), and Ag–In–Mn (15%). In the 2D layered category, only pure Bi-based or pure Sb-based compositions have been reported, with almost an equivalent proportion. Regarding halides, it appears that Cl (83%) and Br (13%) based materials have widely been explored in the context of LED applications, whereas alloys or iodine compositions are rarer. This is quite different from solar cell applications where the iodides are dominant (74%) due to their lower bandgaps capable to harvest low-energy photons. Finally, inorganic cations are by far the most frequent choice for the A site (89%) in LED applications because of their comparatively higher PLQYs, better stability against heating, and slightly lower hygroscopicity. In addition, no organic–inorganic mixtures for the A site are reported so far.

## V. PHOTO-CATALYSIS

The main requirements for a promising photocatalytic material are suitable band alignments and bandgaps, strong light absorption, high chemical stability, efficient charge carrier transport, and good operation in strong acidity and/or alkali environments.<sup>211–213</sup> Over the past few years, the potential of Pb-based halide perovskites has been investigated as a catalyst for photocatalytic hydrogen ( $\text{H}_2$ ) evolution,  $\text{CO}_2$  reduction reaction, and various organic synthesis or chemical reactions.<sup>212,214</sup>

The performance of a complete water splitting system can be evaluated by introducing the solar-to-hydrogen (STH) conversion efficiency.<sup>215</sup> STH has reached nowadays values of 19% close to the theoretical limits (30% under light concentration),<sup>216–218</sup> but progress is needed to significantly lower the cost of the systems and enhance their operational stability.<sup>219</sup> Naturally, halide perovskites appear as low-cost alternative electrical power sources needed for water splitting, thanks to their excellent photovoltaic performances, but single-junction cells made of efficient perovskite materials for photovoltaic (PV) do not usually produce enough voltage to drive simultaneously the hydrogen evolution reaction (HER) or oxygen evolution reaction (OER) in photocatalytic water splitting. This is not the case for perovskite in tandem solar cell configurations with silicon that exhibit nice STH values up to 18.7% but rely on classical electrode materials.<sup>220</sup> On the other hand, Pb-free perovskite solar cells are still far from reaching the efficiency and operational stability under the ambient condition of their Pb-based counterparts and are thus not the best candidates so far as electrical power sources to be included in complete water splitting systems.

Interestingly, perovskite materials can also directly participate in the chemical reactions at the electrodes. This was first shown in 2016 when  $\text{MAPbI}_3$  showed promising performance for photocatalytic water splitting.<sup>221</sup> The  $\text{H}_2$  evolution rate was measured at  $57 \mu\text{mol g}^{-1} \text{h}^{-1}$  with a splitting efficiency of 0.81%.  $\text{MAPbI}_3$  is stable at a specific saturation solution where  $[\text{I}^-] \leq [\text{H}^+]$  and  $\text{pH} \leq -0.5$ . In 2018, Wang *et al.*<sup>222,223</sup> proposed a heterostructure of  $\text{MAPbI}_3/\text{TiO}_2/\text{Pt}$  and  $\text{MAPbI}_3/\text{Ta}_2\text{O}_5/\text{Pt}$  with significant enhancement in the  $\text{H}_2$  evolution rate of 89-fold and 52-fold over  $\text{MAPbI}_3/\text{Pt}$ . From that perspective, Pb-free perovskites may play a more interesting role since the constraint of being an efficient photovoltaic material no longer applies.

**TABLE II.** Overview of various Pb-free halide perovskites used for LED applications. The emission peak positions (in nm), light emission colors, full-width half maxima (FWHM, in nm) of the emissions, and PLQYs (in %) are indicated. Films, powder, nanocrystals (NCs), or more rarely nanoplatelets or nanocages are used. Boldface denotes state of the art results.

Category	Compounds	Emission peak (nm)	Color	FWHM (nm)	PLQY (%)	Comment	Reference
ABX <sub>3</sub>	MASn(Br/I) <sub>3</sub>	667–945	...	...	<5.3	Films	188
	CsSn(Br/I) <sub>3</sub>	667–887	...	...		Films	54
	CsSnBr <sub>3</sub>	670	Dark red	56	2.1	Nanocages	189
	CsSnBr <sub>3</sub>	672	Red	54	9.1	Films	190
	CsSnI <sub>3</sub>	950	Infrared		3.8	Films	191
	CsBr: Eu <sup>2+</sup>	440	White	31	<b>32.8<sup>b</sup></b>	NCs	192
A <sub>2</sub> BB'X <sub>6</sub>	Cs <sub>2</sub> AgBiCl <sub>6</sub>	395	...	68	6.7	NCs	193
		610	...	200	3	Powder	175
	Cs <sub>2</sub> AgBiBr <sub>6</sub>	465	...	82	0.7	NCs	193
	Cs <sub>2</sub> (Na <sub>0.75</sub> Ag <sub>0.25</sub> )BiCl <sub>6</sub>	610	...	160	45	Powder	175
	Cs <sub>2</sub> (Na <sub>0.4</sub> Ag <sub>0.6</sub> )InCl <sub>6</sub> : Bi <sup>3+</sup>	552	White	40.9	86.2	Powder	177
	Cs <sub>2</sub> (Na <sub>0.4</sub> Ag <sub>0.6</sub> )InCl <sub>6</sub> : 5.49% Ho <sup>3+</sup>	490	White		60.5	Powder	194
	Cs <sub>2</sub> Ag(In <sub>0.875</sub> Bi <sub>0.125</sub> )Cl <sub>6</sub>	585	White	...	70.3	Powder	195
	Cs <sub>2</sub> NaBiCl <sub>6</sub>	730	...	...		Powder	181
	Cs <sub>2</sub> NaBiCl <sub>6</sub> : Mn <sup>2+</sup>	590			15	Powder	181
	Cs <sub>2</sub> Na <sub>0.995</sub> Bi <sub>0.995</sub> Mn <sub>0.01</sub> Cl <sub>6</sub>	590	Orange–red	...	11.4	Powder	181
	Cs <sub>2</sub> Na <sub>0.987</sub> Bi <sub>0.987</sub> Mn <sub>0.026</sub> Cl <sub>6</sub>	590	Orange–red	...	12.4	Powder	181
	Cs <sub>2</sub> Na <sub>0.969</sub> Bi <sub>0.969</sub> Mn <sub>0.062</sub> Cl <sub>6</sub>	590	Orange–red	...	15.1	Powder	181
	Cs <sub>2</sub> AgInCl <sub>6</sub>	560	White	...	1.6	NCs	180
		...	...	...	6	NCs	196
	Cs <sub>2</sub> AgBi <sub>0.085</sub> In <sub>0.915</sub> Cl <sub>6</sub>	600	White	200	34	Powder	197
	Cs <sub>2</sub> AgIn <sub>0.9</sub> Cr <sub>0.1</sub> Cl <sub>6</sub>	1010	Near-infrared	180	23.5	Powder	198
	Cs <sub>2</sub> NaInCl <sub>6</sub> : 10% Ag	535	Yellow	...	31.1	NCs	176
	Cs <sub>2</sub> Ag <sub>0.4</sub> Na <sub>0.6</sub> InCl <sub>6</sub>	...	...	...	22	NCs	196
	Cs <sub>2</sub> AgInCl <sub>6</sub> : 0.9% Mn <sup>2+</sup>	632	White	...	3–5	Powder	199
	Cs <sub>2</sub> AgInCl <sub>6</sub> : 0.5% Mn <sup>2+</sup>	620	Orange	...	9	NCs	180
	Cs <sub>2</sub> AgInCl <sub>6</sub> : 1.5% Mn <sup>2+</sup>	620	Orange	...	16	NCs	180
	Cs <sub>2</sub> AgInCl <sub>6</sub> : Mn <sup>2+</sup>	630	...	...	2	Powder	181
	Cs <sub>2</sub> NaInCl <sub>6</sub> : 1% Sb <sup>3+</sup>	445	Blue		82	Powder	185
	Cs <sub>2</sub> KInCl <sub>6</sub> : 5% Sb <sup>3+</sup>	495	Green		<b>93<sup>a</sup></b>	Powder	185
	Cs <sub>2</sub> NaEuCl <sub>6</sub>	593	Red	...	35	Powder	200
	Cs <sub>2</sub> NaTbCl <sub>6</sub>	548	Green	...	56	Powder	200
	A <sub>2</sub> BX <sub>6</sub>	Cs <sub>2</sub> SnCl <sub>6</sub> : 2.75% Bi <sup>3+</sup>	455	White	66	78.9	Powder
Cs <sub>2</sub> SnCl <sub>6</sub> : 1.16% Bi <sup>3+</sup>		457	White	63	68.3	Powder	201
Cs <sub>2</sub> SnCl <sub>6</sub> : 0.11% Bi <sup>3+</sup>		454	White	65	67.6	Powder	201
Cs <sub>2</sub> SnCl <sub>6</sub> : Sb <sup>3+</sup>		602	White	101	37	Powder	202
Cs <sub>2</sub> SnCl <sub>6</sub> : Ce <sup>3+</sup>		455		80	6.57	NCs	203
Cs <sub>2</sub> SnCl <sub>6</sub> : Te <sup>3+</sup>		580	Yellow–green	<100	<b>95.4<sup>d</sup></b>	Powder	186
(NH <sub>4</sub> ) <sub>2</sub> SnCl <sub>6</sub> : 0.5% Te <sup>3+</sup>		590	Orange	127	83.5	Powder	187
Cs <sub>2</sub> SnI <sub>6</sub>		643–742	...	75	28	Nanoplatelets	204
(NH <sub>4</sub> ) <sub>2</sub> SnCl <sub>6</sub>		590	...	127	<0.05	Powder	187
Cs <sub>2</sub> ZrCl <sub>6</sub>		...	...	...	31	Powder	205
Cs <sub>2</sub> ZrCl <sub>6</sub> : Bi <sup>3+</sup>		456	Blue	63	50	Powder	205

TABLE II. (Continued.)

Category	Compounds	Emission peak (nm)	Color	FWHM (nm)	PLQY (%)	Comment	Reference
A <sub>3</sub> B <sub>2</sub> X <sub>9</sub>	Cs <sub>3</sub> Bi <sub>2</sub> Br <sub>9</sub>	410	Blue	48	19.4	NCs	206
	Cs <sub>3</sub> Bi <sub>2</sub> Cl <sub>9</sub>	393	Blue	59	26.4	NCs	206
	Cs <sub>3</sub> Sb <sub>2</sub> Br <sub>9</sub>	410	Blue	41	46	NCs	63
	Cs <sub>3</sub> Sb <sub>2</sub> Cl <sub>9</sub>	370	...	52	11	NCs	63
	Cs <sub>3</sub> Sb <sub>2</sub> I <sub>9</sub>	560	...	56	23	NCs	63
	Cs <sub>3</sub> Sb <sub>2</sub> Br <sub>9</sub>	408	Violet	...	51.2	NCs	207
	FA <sub>3</sub> Bi <sub>2</sub> Br <sub>9</sub>	437	Blue	65	52	NCs	208
	MA <sub>3</sub> Bi <sub>2</sub> Br <sub>9</sub>	430	Blue	62	12	NCs	209
MA <sub>3</sub> Bi <sub>2</sub> (Cl, Br) <sub>9</sub>	422	Blue	41	<b>54.1<sup>a</sup></b>	NCs	210	

<sup>a</sup>The highest value of PLQY for each category of Pb-free perovskites, as highlighted in a bold font.

In the same objective of reducing the use of fossil fuel, the CO<sub>2</sub> reduction has also a very important role to play and it has witnessed significant progress by using perovskite materials. For instance, in 2017, Xu *et al.*<sup>224</sup> used CsPbBr<sub>3</sub> nanocrystals (NCs) as novel photocatalysts for CO<sub>2</sub> reduction at a rate of 23.73 μmol g<sup>-1</sup> h<sup>-1</sup> and up to 29.78 μmol g<sup>-1</sup> h<sup>-1</sup>, with graphene oxide to collect the charge of the CsPbBr<sub>3</sub> NCs. Although Pb-based perovskites are potential candidates for photocatalysts, they are also somehow limited by their low chemical stability.

To ensure the long-term stability of photocathode and photoanode and to avoid Pb contamination during the pre- and post-processing, Pb-free perovskites have been investigated as alternative solutions.<sup>19</sup> Among the technical specifications for an effective photocatalyst, a relatively wide optical bandgap lying in the visible range is ideal for promoting the photocatalytic reaction. Therefore, double perovskites and the 2D perovskite derivatives are of particular interest for such applications. In addition, the high ambient stabilities of these Pb-free materials, compared to conventional 3D perovskites (and especially with respect to Sn<sup>2+</sup> compounds) makes them even more promising. In fact, first-principles calculations<sup>225</sup> predict that most of the Bi/Ag double perovskites have both bandgaps and energy levels that are suitable for photocatalytic water splitting. On the other hand, in order to promote the CO<sub>2</sub> reduction reaction, further chemical engineering is needed to tune the bandgaps of double as well as 2D layered perovskites. For example, the synthesized all-inorganic Pb-free double perovskite Cs<sub>2</sub>AgBiX<sub>6</sub> NCs have their indirect bandgaps decreasing from 2.56 eV when X = Cl to 1.82 eV when X = I.<sup>226</sup> As a result, the Cs<sub>2</sub>AgBiI<sub>6</sub> NCs shows the best photoreduction activity with a CO yield of 18.9 μmol g<sup>-1</sup> under visible light irradiation (λ ≥ 420 nm, 300 W Xe lamp) within 3 h. Similarly, the bandgap of the 2D layered perovskite Cs<sub>3</sub>Bi<sub>2</sub>X<sub>9</sub> NCs decreases from 3.08 to 2.01 eV as halide X goes from Cl<sup>-</sup> to I<sup>-</sup>.<sup>227</sup> The highest CO yielding speed is 54 μmol·g<sup>-1</sup> when X = Br<sub>0.5</sub>I<sub>0.5</sub>, compared to the 48 μmol g<sup>-1</sup> when X = Cl<sub>0.5</sub>Br<sub>0.5</sub> and 11 μmol g<sup>-1</sup> when X = I under visible-light irradiation (λ ≥ 420 nm, 300 W Xe lamp) for 3 h. The suitable band structure, wide light absorption range, large photocurrent, and small impedance of Cs<sub>3</sub>Bi<sub>2</sub>(Br<sub>0.5</sub>I<sub>0.5</sub>)<sub>9</sub> contribute to its greater activity in gas–solid interface than in the majority of the liquid-phase CO<sub>2</sub> reduction systems.

Table III lists photocatalytic applications of different types of Pb-free perovskites and the yielding speed (in μmol g<sup>-1</sup> h<sup>-1</sup>) concerning CO<sub>2</sub> reduction into CO and/or CH<sub>4</sub> and H<sub>2</sub> evolution. In double perovskites, the Cs<sub>2</sub>AgBiBr<sub>6</sub> nanoplatelets show the best performance for CO<sub>2</sub> reduction.<sup>228</sup> Within 6 h, these nanoplatelets have a total electron consumption eightfold higher than that of Cs<sub>2</sub>AgBiBr<sub>6</sub> NCs, namely, 255.4 vs 30.8 μmol g<sup>-1</sup>. This large increase can be explained by the anisotropic confinement of charge carriers and the in-plane long diffusion length in nanoplatelets.<sup>229–231</sup> In order to further improve H<sub>2</sub> production, Jiang *et al.*<sup>232</sup> have synthesized successfully a composite of Cs<sub>2</sub>AgBiBr<sub>6</sub> supported on nitrogen-doped carbon materials (N–C). This heterostructure Cs<sub>2</sub>AgBiBr<sub>6</sub>/N–C has a speed almost 20-fold faster than the pure Cs<sub>2</sub>AgBiBr<sub>6</sub>. In 2D layered perovskite photocatalysts, their surface activities are strongly dominated by the defects/traps. For example, the Cs<sub>3</sub>Sb<sub>2</sub>Br<sub>9</sub> NCs exhibit the highest CO yield of 127.5 μmol g<sup>-1</sup> h<sup>-1</sup> to date.<sup>233</sup> One explanation is the existence of Sb on their surfaces, which leads to a great improvement of the reactivity. This is in contrast to the nonreactive surfaces of the Pb based perovskites.

Although 3D perovskites are not the most popular for photocatalytic applications, several breakthroughs are still made by using the high hydrophobic dimethylammonium (DMA = CH<sub>3</sub>NH<sub>2</sub>CH<sub>3</sub><sup>+</sup>) as the A site cation. In 2021, Romani *et al.*<sup>234</sup> have successfully integrated DMASnX<sub>3</sub> with the graphitic carbon nitride (g-C<sub>3</sub>N<sub>4</sub>), forming the DMASnBr<sub>3</sub>@g-C<sub>3</sub>N<sub>4</sub>. Thanks to the efficient transport of charge carriers, its highest rate of H<sub>2</sub> production in deionized water reaches 1730 μmol g<sup>-1</sup> h<sup>-1</sup>, which is much higher than the 6.0 μmol g<sup>-1</sup> h<sup>-1</sup> of pure DMASnBr<sub>3</sub> and 2.0 μmol g<sup>-1</sup> h<sup>-1</sup> of pure g-C<sub>3</sub>N<sub>4</sub>. The small differences in interfacial energy between CBM of DMASnBr<sub>3</sub> and H<sup>+</sup>/H<sub>2</sub> reduction potential and between VBM of g-C<sub>3</sub>N<sub>4</sub> and triethanolamine oxidation potential are proposed to contribute to a large nonadiabatic charge transfer between DMASnBr<sub>3</sub> and g-C<sub>3</sub>N<sub>4</sub>,<sup>235</sup> and in turn the high photocatalytic yield.

It should be mentioned that apart from the CO<sub>2</sub> reduction reaction and H<sub>2</sub> production, the double and 2D layered perovskites also show potential for more complex reactions involving the transformation of one molecule into another (for clarity they are not listed in Table III).<sup>236</sup> For example, the Cs<sub>2</sub>AgBiBr<sub>6</sub> NCs can degrade 97% of toxic NO gas within 30 min and maintain stability in four

**TABLE III.** Overview of the various Pb-free halide perovskites used for photocatalytic applications. Boldface denotes state of the art results.

Category	Compounds	Yielding of main product ( $\mu\text{mol g}^{-1} \text{h}^{-1}$ )			Reference
		CO	CH <sub>4</sub>	H <sub>2</sub>	
ABX <sub>3</sub>	DMASnI <sub>3</sub>			0.64	240
	DMASnBr <sub>3</sub>			6	241
	DMASnBr <sub>3</sub> + 10% triethanolamine + 1 wt. % Pt			11	241
	DMASnBr <sub>3</sub> + 10% triethanolamine + 3 wt. % Pt			6	234
	DMASnBr <sub>3</sub> @C <sub>3</sub> N <sub>4</sub> -33% + 10% triethanolamine + 3 wt. % Pt			<b>1730<sup>a</sup></b>	234
A <sub>2</sub> BB'X <sub>6</sub>	Cs <sub>2</sub> AgBiBr <sub>6</sub> (NCs)	0.92	0.11		242
	Cs <sub>2</sub> AgBiBr <sub>6</sub> (washed NCs)	2.35	0.16		242
	Cs <sub>2</sub> AgBiBr <sub>6</sub> (bulk)	0.37	0.02		242
	Cs <sub>2</sub> AgBiI <sub>6</sub> (NCs)	6.3			226
	Cs <sub>2</sub> AgBi(Br <sub>0.5</sub> I <sub>0.5</sub> ) <sub>6</sub> (NCs)	3.93			226
	Cs <sub>2</sub> AgBiCl <sub>6</sub> (NCs)	4.54			226
	Cs <sub>2</sub> AgBiBr <sub>6</sub> @C <sub>3</sub> N <sub>4</sub> -10%	~1.8	~0.2		243
	Cs <sub>2</sub> AgBiBr <sub>6</sub> @C <sub>3</sub> N <sub>4</sub> -82%	~0.66	~1.54		243
	Cs <sub>2</sub> AgBiBr <sub>6</sub> (nanocubes)	3.8	1.3		228
	Cs <sub>2</sub> AgBiBr <sub>6</sub> (nanoplatelets)	<b>28.1<sup>a</sup></b>	<b>14.5<sup>a</sup></b>		228
	Cs <sub>2</sub> AgBiBr <sub>6</sub> /N-C			<b>380<sup>a</sup></b>	232
	Cs <sub>2</sub> AgBiBr <sub>6</sub>			20	232
	Cs <sub>2</sub> AgBiBr <sub>6</sub> /RGO			48.9	244
	Cs <sub>2</sub> AgBiBr <sub>6</sub> (bulk)			0.077	245
	Cs <sub>2</sub> AgBiBr <sub>6</sub> (defect-rich)			0.406	245
Cs <sub>2</sub> AgBiBr <sub>6</sub> /Pt			0.733	245	
Cs <sub>2</sub> AgBiBr <sub>6</sub> /Mo <sub>3</sub> S <sub>13</sub> <sup>2-</sup>			2.47	245	
A <sub>3</sub> B <sub>2</sub> X <sub>9</sub>	Cs <sub>3</sub> Sb <sub>2</sub> Br <sub>9</sub>	<b>127.5<sup>a</sup></b>			233
	Cs <sub>3</sub> Sb <sub>2</sub> I <sub>9</sub> (microblocks)	2.4			246
	Cs <sub>3</sub> Sb <sub>2</sub> I <sub>9</sub> (microclusters)	1.7			246
	Cs <sub>3</sub> Sb <sub>2</sub> I <sub>9</sub>	92.8	2.9	10.4	247
	Cs <sub>3</sub> Bi <sub>2</sub> Cl <sub>9</sub>	21.01			248
	Cs <sub>3</sub> Bi <sub>2</sub> Br <sub>9</sub>	26.95			248
	Cs <sub>3</sub> Bi <sub>2</sub> (Br <sub>0.5</sub> I <sub>0.5</sub> ) <sub>9</sub>	18			227
	Cs <sub>3</sub> Bi <sub>2</sub> (Cl <sub>0.5</sub> Br <sub>0.5</sub> ) <sub>9</sub>	16			227
	Cs <sub>3</sub> Bi <sub>2</sub> I <sub>9</sub>	7.76	1.49		249
	Rb <sub>3</sub> Bi <sub>2</sub> I <sub>9</sub>	1.82	1.70		249
	MA <sub>3</sub> Bi <sub>2</sub> I <sub>9</sub>	0.72	0.98		249
	Cs <sub>3</sub> Bi <sub>2</sub> I <sub>9</sub> (QDs)			32.21	250
	Cs <sub>3</sub> Bi <sub>2</sub> I <sub>9</sub> @NH <sub>2</sub> -UiO-66			141.87	250
MA <sub>3</sub> Bi <sub>2</sub> I <sub>9</sub>			<b>169.21<sup>a</sup></b>	251	
Cs <sub>3</sub> Bi <sub>0.6</sub> Sb <sub>1.4</sub> I <sub>9</sub>			926	252	

<sup>a</sup>The highest value of product yielding rate for each category of Pb-free perovskites, as highlighted in a bold font.

runs of photocatalytic reaction.<sup>237</sup> An almost complete degradation (~98%) of Rhodamine B is obtained by Cs<sub>2</sub>AgBiBr<sub>6</sub> photocatalysis during 120 min under continuous irradiation.<sup>238</sup> Cs<sub>2</sub>AgInCl<sub>6</sub> particles degrade ~98.5% of the water-insoluble carcinogen Sudan Red III in just 16 min and have good stability for five cycle operations.<sup>236</sup> In 2020, (MA<sub>x</sub>Cs<sub>1-x</sub>)<sub>3</sub>SbBr<sub>9</sub> was used for the first time for the activation of C-H bonds, with improved photocatalytic performance, thanks to the substitution of MA by Cs.<sup>239</sup> This unique effect of the A site cation tuning is proposed to stem from the octahedron distortion

induced by the A cation, which changes not only the electronic properties of the X anions but also the electron transfer from molecules to Br sites.

The summary of various types of Pb-free materials employed so far for photo-catalytic applications is further reported in Fig. 2(c). Double (45%) and 2D layered perovskites (41%) are predominant. The remaining 14% are conventional single ABX<sub>3</sub> Pb-free halide perovskites that have been solely used for the photocatalysis of H<sub>2</sub>. Obviously, vacancy ordered Pb-free halide perovskites have not yet

been explored for photocatalysis. In the conventional and double perovskites, all the B site cations are Sn and Ag–Bi, respectively. Instead, in 2D layered perovskites, 66% of the explored site B cations are based on pure Bi, 27% on pure Sb, and the remaining 7% on a mixture of both cations. As the material needs to absorb visible light efficiently, metal halides based on Br (54%) and I (33%) are most often used for photocatalytic applications. As for LEDs, most of the A site cations employed in Pb-free perovskites used as photocatalysts are inorganic (81%). To be noted, compositions with mixed organic-inorganic A site cations have not been reported so far.

## VI. CONCLUSION

This Perspective reports on the state-of-the-art of Pb-free halide perovskite semiconductors for optoelectronic applications, focusing on solar cells, LEDs, and photocatalysts. Clearly, Sn-based halide perovskites are the most explored and performant for photovoltaic applications. On the other hand, Bi, Ag, and Sb atoms are predominant in the composition of photocatalysts, whereas for LEDs many more metallic cations have been explored with the prevalence of alloys.

For solar cell applications, the PCE achieved to date for any of the double perovskites  $A_2BB'X_6$ , vacancy ordered double perovskites  $A_2BX_6$ , or 2D perovskite derivatives  $A_3B_2X_9$  is below 4% and thus far away from the 25.8% achieved with Pb-based halide perovskites.<sup>10</sup> Tin-iodides  $ASnI_3$  compositions are the most promising with a current record reaching 14.6%.<sup>79</sup> They also allow room for improvements given that the predicted theoretical limit for thick layers under AM1.5G illumination for stannates is as high as 32.3%.<sup>83</sup> The materials are less stable than their Pb-based counterparts when subjected to ambient conditions due to the fast  $Sn^{2+}$  oxidation. Yet, a remarkable improvement was achieved recently with over 1300 h of operational stability in  $N_2$ , thanks to chemical engineering by combining the addition of a secondary ammonium salt with that of an effective reducing agent.<sup>80</sup> In addition, Sn/Ge mixed perovskite absorbers also demonstrate improved stability, but their PCE needs to be significantly enhanced. Noteworthy, due to their low electronic bandgap, the Sn-based iodide perovskites can become cornerstone materials and pave the way for tandem perovskite/perovskite solar cells or applications based on low bandgaps.<sup>253,254</sup>

For LED applications, Pb-free halide perovskite materials, in particular,  $A_2BB'X_6$  double perovskite and  $A_2BX_6$  vacancy ordered double perovskite show great promise, especially for white light emission. Indeed, their PLQYs for the white color emission are higher than 78% and those for other colors are remarkably high with some of them higher than 93%. More precisely, 93% for the green emission when  $B = In/Sb$  mixture and  $B' = K$  in  $A_2BB'X_6$  and 95.4% for the yellow–green emission when  $B = Sn/Te$  mixture in  $A_2BX_6$ . Noteworthy, these attractive PLQYs are just one of many features needed to make efficient LEDs. Interface related issues are anticipated to be one of the key factors that limit the potential of lead-free perovskites for photovoltaic applications.

Finally, the Pb-free halide double perovskites and 2D layered perovskites are also promising in the field of photocatalysis due to their large electronic bandgap and stability.<sup>211</sup> For instance, Zhou *et al.* synthesized  $Cs_2AgBiBr_6$  nanocrystals that were shown to be stable for more than three weeks in a low polarity medium under

light-soaking and 55% relative humidity.<sup>242</sup> Double perovskites with  $B = Bi$  and  $B' = Ag$  have the highest rate of  $H_2$  evolution that reaches  $380 \mu\text{mol g}^{-1} \text{h}^{-1}$  when supported on carbon doped with nitrogen.<sup>232</sup> More recently, an impressive hydrogen evolution rate over  $1700 \mu\text{mol g}^{-1} \text{h}^{-1}$  was achieved with the use of the  $ABX_3$   $DMASnBr_3$  and  $g\text{-C}_3\text{N}_4$ , thanks to the favorable alignment of the interfacial energy levels. Regarding  $CO_2$  reduction, the highest rate reported so far with Pb-free halide perovskite catalysts amounts to  $127.5 \mu\text{mol g}^{-1} \text{h}^{-1}$  and uses the layered  $Cs_3Sb_2Br_9$  material. This type of development is still in its infancy and Pb-free metal halide perovskites show great potential as catalytically active materials, especially in the form of nanocrystals such as nanoplatelets, which offer desirable features such as exposed facets.

## ACKNOWLEDGMENTS

This project received funding from the European Union's Horizon 2020 Research and Innovation Program [Grant Agreement Nos. 862656 (DROP-IT) and 861985 (PeroCUBE)]. G.V. acknowledges funding from the Chaire de Recherche Rennes Metropole project. J.E. acknowledges financial support from the Institut Universitaire de France.

## AUTHOR DECLARATIONS

### Conflict of Interest

The authors have no conflicts to disclose.

## DATA AVAILABILITY

The data that support the findings of this study are available within the article.

## REFERENCES

- 1 S. D. Stranks and H. J. Snaith, *Nat. Nanotechnol.* **10**, 391 (2015).
- 2 M. A. Green, A. Ho-Baillie, and H. J. Snaith, *Nat. Photonics* **8**, 506 (2014).
- 3 K. Lin, J. Xing, L. N. Quan, F. P. G. de Arquer, X. Gong, J. Lu, L. Xie, W. Zhao, D. Zhang, C. Yan, W. Li, X. Liu, Y. Lu, J. Kirman, E. H. Sargent, Q. Xiong, and Z. Wei, *Nature* **562**, 245 (2018).
- 4 K. S. Schanze, P. V. Kamat, P. Yang, and J. Bisquert, *ACS Energy Lett.* **5**, 2602 (2020).
- 5 A. Kojima, K. Teshima, Y. Shirai, and T. Miyasaka, *J. Am. Chem. Soc.* **131**, 6050 (2009).
- 6 S. De Wolf, J. Holovsky, S.-J. Moon, P. Löper, B. Niesen, M. Ledinsky, F.-J. Haug, J.-H. Yum, and C. Ballif, *J. Phys. Chem. Lett.* **5**, 1035 (2014).
- 7 S. D. Stranks, G. E. Eperon, G. Grancini, C. Menelaou, M. J. P. Alcocer, T. Leijtens, L. M. Herz, A. Petrozza, and H. J. Snaith, *Science* **342**, 341 (2013).
- 8 D. Shi, V. Adinolfi, R. Comin, M. Yuan, E. Alarousu, A. Buin, Y. Chen, S. Hoogland, A. Rothenberger, K. Katsiev, Y. Losovyj, X. Zhang, P. A. Dowben, O. F. Mohammed, E. H. Sargent, and O. M. Bakr, *Science* **347**, 519 (2015).
- 9 M. Abdi-Jalebi, Z. Andaji-Garmaroudi, S. Cacovich, C. Stavrakas, B. Philippe, J. M. Richter, M. Alsari, E. P. Booker, E. M. Hutter, A. J. Pearson, S. Lilliu, T. J. Savenije, H. Rensmo, G. Divitini, C. Ducati, R. H. Friend, and S. D. Stranks, *Nature* **555**, 497 (2018).
- 10 H. Min, D. Y. Lee, J. Kim, G. Kim, K. S. Lee, J. Kim, M. J. Paik, Y. K. Kim, K. S. Kim, M. G. Kim, T. J. Shin, and S. Il Seok, *Nature* **598**, 444 (2021).
- 11 A. Babayigit, A. Ethirajan, M. Muller, and B. Conings, *Nat. Mater.* **15**, 247 (2016).

- <sup>12</sup>S.-Y. Bae, S. Y. Lee, J.-w. Kim, H. N. Umh, J. Jeong, S. Bae, J. Yi, Y. Kim, and J. Choi, *Sci. Rep.* **9**, 4242 (2019).
- <sup>13</sup>J. Li, H.-L. Cao, W.-B. Jiao, Q. Wang, M. Wei, I. Cantone, J. Lü, and A. Abate, *Nat. Commun.* **11**, 310 (2020).
- <sup>14</sup>C. Ponti, G. Nasti, D. Di Girolamo, I. Cantone, F. A. Alharthi, and A. Abate, *Trends Ecol. Evol.* **37**, 281 (2022).
- <sup>15</sup>A. Exrance, *Nature* **570**, 429 (2019).
- <sup>16</sup>T. A. Berhe, W.-N. Su, C.-H. Chen, C.-J. Pan, J.-H. Cheng, H.-M. Chen, M.-C. Tsai, L.-Y. Chen, A. A. Dubale, and B.-J. Hwang, *Energy Environ. Sci.* **9**, 323 (2016).
- <sup>17</sup>J. S. Manser, M. I. Saidaminov, J. A. Christians, O. M. Bakr, and P. V. Kamat, *Acc. Chem. Res.* **49**, 330 (2016).
- <sup>18</sup>W. Ke, C. C. Stoumpos, and M. G. Kanatzidis, *Adv. Mater.* **31**, 1803230 (2019).
- <sup>19</sup>C. Pareja-Rivera, D. Morett, D. Barreiro-Argüelles, P. Olalde-Velasco, and D. Solis-Ibarra, *J. Phys. Energy* **3**, 032014 (2021).
- <sup>20</sup>Q. A. Akkerman and L. Manna, *ACS Energy Lett.* **5**, 604 (2020).
- <sup>21</sup>S. Boyer-Richard, C. Katan, B. Traoré, R. Scholz, J.-M. Jancu, and J. Even, *J. Phys. Chem. Lett.* **7**, 3833 (2016).
- <sup>22</sup>I. Chung, J.-H. Song, J. Im, J. Androulakis, C. D. Malliakas, H. Li, A. J. Freeman, J. T. Kenney, and M. G. Kanatzidis, *J. Am. Chem. Soc.* **134**, 8579 (2012).
- <sup>23</sup>C. C. Stoumpos, C. D. Malliakas, and M. G. Kanatzidis, *Inorg. Chem.* **52**, 9019 (2013).
- <sup>24</sup>F. Hao, C. C. Stoumpos, D. H. Cao, R. P. H. Chang, and M. G. Kanatzidis, *Nat. Photonics* **8**, 489 (2014).
- <sup>25</sup>N. K. Noel, S. D. Stranks, A. Abate, C. Wehrenfennig, S. Guarnera, A.-A. Haghighirad, A. Sadhanala, G. E. Eperon, S. K. Pathak, M. B. Johnston, A. Petrozza, L. M. Herz, and H. J. Snaith, *Energy Environ. Sci.* **7**, 3061 (2014).
- <sup>26</sup>S. Gupta, D. Cahen, and G. Hodes, *J. Phys. Chem. C* **122**, 13926 (2018).
- <sup>27</sup>X. Meng, Y. Wang, J. Lin, X. Liu, X. He, J. Barbaud, T. Wu, T. Noda, X. Yang, and L. Han, *Joule* **4**, 902 (2020).
- <sup>28</sup>A. Kaltzoglou, G. K. Manolis, M. M. Elsenety, I. Koutselas, V. Psycharis, A. G. Kontos, and P. Falaras, *J. Electron. Mater.* **48**, 7533 (2019).
- <sup>29</sup>W. Ke, C. C. Stoumpos, M. Zhu, L. Mao, I. Spanopoulos, J. Liu, O. Y. Kontsevoi, M. Chen, D. Sarma, Y. Zhang, M. R. Wasielewski, and M. G. Kanatzidis, *Sci. Adv.* **3**, e1701293 (2017).
- <sup>30</sup>C. C. Stoumpos, L. Frazer, D. J. Clark, Y. S. Kim, S. H. Rhim, A. J. Freeman, J. B. Ketterson, J. I. Jang, and M. G. Kanatzidis, *J. Am. Chem. Soc.* **137**, 6804 (2015).
- <sup>31</sup>G. E. Eperon, T. Leijtens, K. A. Bush, R. Prasanna, T. Green, J. T.-W. Wang, D. P. McMeehin, G. Volonakis, R. L. Milot, R. May, A. Palmstrom, D. J. Slotcavage, R. A. Belisle, J. B. Patel, E. S. Parrott, R. J. Sutton, W. Ma, F. Moghadam, B. Conings, A. Babayigit, H.-G. Boyen, S. Bent, F. Giustino, L. M. Herz, M. B. Johnston, M. D. McGehee, and H. J. Snaith, *Science* **354**, 861 (2016).
- <sup>32</sup>M. Chen, M.-G. Ju, H. F. Garces, A. D. Carl, L. K. Ono, Z. Hawash, Y. Zhang, T. Shen, Y. Qi, R. L. Grimm, D. Pacifici, X. C. Zeng, Y. Zhou, and N. P. Padture, *Nat. Commun.* **10**, 16 (2019).
- <sup>33</sup>S. Shao, J. Liu, G. Portale, H.-H. Fang, G. R. Blake, G. H. ten Brink, L. J. A. Koster, and M. A. Loi, *Adv. Energy Mater.* **8**, 1702019 (2017).
- <sup>34</sup>J. Dong, S. Shao, S. Kahmann, A. J. Rommens, D. Hermida-Merino, G. H. ten Brink, M. A. Loi, and G. Portale, *Adv. Funct. Mater.* **30**, 2001294 (2020).
- <sup>35</sup>C. W. Cross and W. F. Hillebrand, *Am. J. Sci.* **s3-26**, 271 (1883).
- <sup>36</sup>A. H. Slavney, T. Hu, A. M. Lindenberg, and H. I. Karunadasa, *J. Am. Chem. Soc.* **138**, 2138 (2016).
- <sup>37</sup>E. T. McClure, M. R. Ball, W. Windl, and P. M. Woodward, *Chem. Mater.* **28**, 1348 (2016).
- <sup>38</sup>G. Volonakis, M. R. Filip, A. A. Haghighirad, N. Sakai, B. Wenger, H. J. Snaith, and F. Giustino, *J. Phys. Chem. Lett.* **7**, 1254 (2016).
- <sup>39</sup>G. Volonakis, A. A. Haghighirad, R. L. Milot, W. H. Sio, M. R. Filip, B. Wenger, M. B. Johnston, L. M. Herz, H. J. Snaith, and F. Giustino, *J. Phys. Chem. Lett.* **8**, 772 (2017).
- <sup>40</sup>A. H. Slavney, L. Leppert, A. Saldivar Valdes, D. Bartesaghi, T. J. Savenije, J. B. Neaton, and H. I. Karunadasa, *Angew. Chem., Int. Ed.* **57**, 12765 (2018).
- <sup>41</sup>G. Volonakis, A. A. Haghighirad, H. J. Snaith, and F. Giustino, *J. Phys. Chem. Lett.* **8**, 3917 (2017).
- <sup>42</sup>F. Wei, Z. Deng, S. Sun, N. T. P. Hartono, H. L. Seng, T. Buonassisi, P. D. Bristowe, and A. K. Cheetham, *Chem. Commun.* **55**, 3721 (2019).
- <sup>43</sup>F. Wei, Z. Deng, S. Sun, F. Xie, G. Kieslich, D. M. Evans, M. A. Carpenter, P. D. Bristowe, and A. K. Cheetham, *Mater. Horiz.* **3**, 328 (2016).
- <sup>44</sup>M. R. Filip, S. Hillman, A. A. Haghighirad, H. J. Snaith, and F. Giustino, *J. Phys. Chem. Lett.* **7**, 2579 (2016).
- <sup>45</sup>B. A. Connor, R.-I. Biega, L. Leppert, and H. I. Karunadasa, *Chem. Sci.* **11**, 7708 (2020).
- <sup>46</sup>Z. Deng, F. Wei, S. Sun, G. Kieslich, A. K. Cheetham, and P. D. Bristowe, *J. Mater. Chem. A* **4**, 12025 (2016).
- <sup>47</sup>A. H. Slavney, L. Leppert, D. Bartesaghi, A. Gold-Parker, M. F. Toney, T. J. Savenije, J. B. Neaton, and H. I. Karunadasa, *J. Am. Chem. Soc.* **139**, 5015 (2017).
- <sup>48</sup>G. Volonakis, N. Sakai, H. J. Snaith, and F. Giustino, *J. Phys. Chem. Lett.* **10**, 1722 (2019).
- <sup>49</sup>E. A. Pogue, J. Bond, C. Imperato, J. B. S. Abraham, N. Drichko, and T. M. McQueen, *J. Am. Chem. Soc.* **143**, 19033 (2021).
- <sup>50</sup>B. Vargas, E. Ramos, E. Pérez-Gutiérrez, J. C. Alonso, and D. Solis-Ibarra, *J. Am. Chem. Soc.* **139**, 9116 (2017).
- <sup>51</sup>B. Vargas, G. Rodríguez-López, and D. Solis-Ibarra, *ACS Energy Lett.* **5**, 3591 (2020).
- <sup>52</sup>M. Liu, S. K. Matta, H. Ali-Löyty, A. Matuhina, G. K. Grandhi, K. Lahtonen, S. P. Russo, and P. Vivo, *Nano Lett.* **22**, 311 (2022).
- <sup>53</sup>B. Vargas, D. T. Reyes-Castillo, E. Coutino-Gonzalez, C. Sánchez-Aké, C. Ramos, C. Falcony, and D. Solis-Ibarra, *Chem. Mater.* **32**, 9307 (2020).
- <sup>54</sup>W. L. Hong, P. H. Lo, H. Z. Chiu, S. F. Horng, and Y. C. Chao, *Adv. Mater. Interfaces* **8**, 2002240 (2021).
- <sup>55</sup>S. Ullah, J. Wang, M. H. Alvi, R. Chang, P. Yang, L. Liu, S. E. Yang, T. Xia, H. Guo, and Y. Chen, *Int. J. Energy Res.* **45**, 1720 (2021).
- <sup>56</sup>B. Lee, C. C. Stoumpos, N. Zhou, F. Hao, C. Malliakas, C.-Y. Yeh, T. J. Marks, M. G. Kanatzidis, and R. P. H. Chang, *J. Am. Chem. Soc.* **136**, 15379 (2014).
- <sup>57</sup>A. E. Maughan, A. M. Ganose, M. M. Bordelon, E. M. Miller, D. O. Scanlon, and J. R. Neilson, *J. Am. Chem. Soc.* **138**, 8453 (2016).
- <sup>58</sup>N. Sakai, A. A. Haghighirad, M. R. Filip, P. K. Nayak, S. Nayak, A. Ramadan, Z. Wang, F. Giustino, and H. J. Snaith, *J. Am. Chem. Soc.* **139**, 6030 (2017).
- <sup>59</sup>Q. Mahmood, M. Hassan, N. Yousaf, A. A. AlObaid, T. I. Al-Muhimeed, M. Morsi, H. Albalawi, and O. A. Alamri, *Mater. Sci. Semicond. Process.* **137**, 106180 (2022).
- <sup>60</sup>H. A. Evans, D. H. Fabini, J. L. Andrews, M. Koerner, M. B. Preefer, G. Wu, F. Wudl, A. K. Cheetham, and R. Seshadri, *Inorg. Chem.* **57**, 10375 (2018).
- <sup>61</sup>C. Wu, F. Guo, L. Zhuang, X. Ai, F. Zhong, H. Yang, and J. Qian, *ACS Energy Lett.* **5**, 1644 (2020).
- <sup>62</sup>B. Cucco, G. Boudier, L. Pedesseau, C. Katan, J. Even, M. Kepenekian, and G. Volonakis, *Appl. Phys. Lett.* **119**, 181903 (2021).
- <sup>63</sup>J. Zhang, Y. Yang, H. Deng, U. Farooq, X. Yang, J. Khan, J. Tang, and H. Song, *ACS Nano* **11**, 9294 (2017).
- <sup>64</sup>F. Lazarini, *Acta Crystallogr., Sect. B: Struct. Crystallogr. Cryst. Chem.* **33**, 2961 (1977).
- <sup>65</sup>A. V. Arakcheeva, M. Bonin, G. Chapuis, and A. I. Zaitsev, *Z. Kristallogr. - Cryst. Mater.* **214**, 279 (1999).
- <sup>66</sup>B. Chabot and E. Parthé, *Acta Crystallogr., Sect. B: Struct. Crystallogr. Cryst. Chem.* **34**, 645 (1978).
- <sup>67</sup>K. Yamada, H. Sera, S. Sawada, H. Tada, T. Okuda, and H. Tanaka, *J. Solid State Chem.* **134**, 319 (1997).
- <sup>68</sup>S.-Y. Kim, Y. Yun, S. Shin, J. H. Lee, Y.-W. Heo, and S. Lee, *Scr. Mater.* **166**, 107 (2019).
- <sup>69</sup>M. Xia, J. H. Yuan, G. Niu, X. Du, L. Yin, W. Pan, J. Luo, Z. Li, H. Zhao, K. H. Xue, X. Miao, and J. Tang, *Adv. Funct. Mater.* **30**, 1910648 (2020).
- <sup>70</sup>B. Lee, J. He, R. P. Chang, and M. G. Kanatzidis, *Nature* **485**, 486 (2012).
- <sup>71</sup>M. M. Lee, J. Teuscher, T. Miyasaka, T. N. Murakami, and H. J. Snaith, *Science* **338**, 643 (2012).
- <sup>72</sup>H.-S. Kim, C.-R. Lee, J.-H. Im, K.-B. Lee, T. Moehl, A. Marchioro, S.-J. Moon, R. Humphry-Baker, J.-H. Yum, J. E. Moser, M. Grätzel, and N.-G. Park, *Sci. Rep.* **2**, 591 (2012).
- <sup>73</sup>P. Tockhorn, J. Sutter, A. Cruz, P. Wagner, K. Jäger, D. Yoo, F. Lang, M. Grischek, B. Li, A. Al-Ashouri, E. Köhnen, M. Stollerfoht, D. Neher, R. Schlattmann, B. Rech, B. Stannowski, S. Albrecht, and C. Becker, "Nano-optical

- designs enhance monolithic perovskite/silicon tandem solar cells toward 29.8% efficiency," *Nat. Portfolio* (published online) (2022).
- <sup>74</sup>H. Tsai, W. Nie, J.-C. Blancon, C. C. Stoumpos, R. Asadpour, B. Harutyunyan, A. J. Neukirch, R. Verduzco, J. J. Crochet, S. Tretiak, L. Pedesseau, J. Even, M. A. Alam, G. Gupta, J. Lou, P. M. Ajayan, M. J. Bedzyk, M. G. Kanatzidis, and A. D. Mohite, *Nature* **536**, 312 (2016).
- <sup>75</sup>L. Mao, C. C. Stoumpos, and M. G. Kanatzidis, *J. Am. Chem. Soc.* **141**, 1171 (2018).
- <sup>76</sup>K. Nishimura, M. A. Kamarudin, D. Hirotani, K. Hamada, Q. Shen, S. Iikubo, T. Minemoto, K. Yoshino, and S. Hayase, *Nano Energy* **74**, 104858 (2020).
- <sup>77</sup>T. Ye, X. Wang, K. Wang, S. Ma, D. Yang, Y. Hou, J. Yoon, K. Wang, and S. Priya, *ACS Energy Lett.* **6**, 1480 (2021).
- <sup>78</sup>C. Wang, Y. Zhang, F. Gu, Z. Zhao, H. Li, H. Jiang, Z. Bian, and Z. Liu, *Matter* **4**, 709 (2021).
- <sup>79</sup>X. Jiang, H. Li, Q. Zhou, Q. Wei, M. Wei, L. Jiang, Z. Wang, Z. Peng, F. Wang, Z. Zang, K. Xu, Y. Hou, S. Teale, W. Zhou, R. Si, X. Gao, E. H. Sargent, and Z. Ning, *J. Am. Chem. Soc.* **143**, 10970 (2021).
- <sup>80</sup>J. Sanchez-Diaz, R. S. Sánchez, S. Masi, M. Krečmarová, A. O. Alvarez, E. M. Barea, J. Rodriguez-Romero, V. S. Chirvony, J. F. Sánchez-Royo, J. P. Martínez-Pastor, and I. Mora-Seró, *Joule* **6**, 861 (2022).
- <sup>81</sup>L.-J. Chen, C.-R. Lee, Y.-J. Chuang, Z.-H. Wu, and C. Chen, *J. Phys. Chem. Lett.* **7**, 5028 (2016).
- <sup>82</sup>P. Wang, F. Li, K. J. Jiang, Y. Zhang, H. Fan, Y. Zhang, Y. Miao, J. H. Huang, C. Gao, X. Zhou, F. Wang, L. M. Yang, C. Zhan, and Y. Song, *Adv. Sci.* **7**, 1903047 (2020).
- <sup>83</sup>A. Filippetti, S. Kahmann, C. Caddeo, A. Mattoni, M. Saba, A. Bosin, and M. A. Loi, *J. Mater. Chem. A* **9**, 11812 (2021).
- <sup>84</sup>B. Li, H. Di, B. Chang, R. Yin, L. Fu, Y. N. Zhang, and L. Yin, *Adv. Funct. Mater.* **31**, 2007447 (2021).
- <sup>85</sup>E. Jökar, C.-H. Chien, C.-M. Tsai, A. Fathi, and E. W.-G. Diau, *Adv. Mater.* **31**, 1804835 (2019).
- <sup>86</sup>Q. Zeng, X. Zhang, X. Feng, S. Lu, Z. Chen, X. Yong, S. A. T. Redfern, H. Wei, H. Wang, H. Shen, W. Zhang, W. Zheng, H. Zhang, J. S. Tse, and B. Yang, *Adv. Mater.* **30**, 1705393 (2018).
- <sup>87</sup>F. Li, C. Zhang, J. H. Huang, H. Fan, H. Wang, P. Wang, C. Zhan, C. M. Liu, X. Li, L. M. Yang, Y. Song, and K. J. Jiang, *Angew. Chem., Int. Ed.* **58**, 6688 (2019).
- <sup>88</sup>F. Hao, C. C. Stoumpos, R. P. H. Chang, and M. G. Kanatzidis, *J. Am. Chem. Soc.* **136**, 8094 (2014).
- <sup>89</sup>T.-B. Song, T. Yokoyama, C. C. Stoumpos, J. Logsdon, D. H. Cao, M. R. Wasielewski, S. Aramaki, and M. G. Kanatzidis, *J. Am. Chem. Soc.* **139**, 836 (2017).
- <sup>90</sup>F. Hao, C. C. Stoumpos, P. Guo, N. Zhou, T. J. Marks, R. P. H. Chang, and M. G. Kanatzidis, *J. Am. Chem. Soc.* **137**, 11445 (2015).
- <sup>91</sup>T. Fujihara, S. Terakawa, T. Matsushima, C. Qin, M. Yahiro, and C. Adachi, *J. Mater. Chem. C* **5**, 1121 (2017).
- <sup>92</sup>T. Handa, T. Yamada, H. Kubota, S. Ise, Y. Miyamoto, and Y. Kanemitsu, *J. Phys. Chem. C* **121**, 16158 (2017).
- <sup>93</sup>T. Yokoyama, D. H. Cao, C. C. Stoumpos, T.-B. Song, Y. Sato, S. Aramaki, and M. G. Kanatzidis, *J. Phys. Chem. Lett.* **7**, 776 (2016).
- <sup>94</sup>M.-C. Jung, S. R. Raga, and Y. Qi, *RSC Adv.* **6**, 2819 (2016).
- <sup>95</sup>E. Greul, P. Docampo, and T. Bein, *Z. Anorg. Allg. Chem.* **643**, 1704 (2017).
- <sup>96</sup>C.-M. Tsai, N. Mohanta, C.-Y. Wang, Y.-P. Lin, Y.-W. Yang, C.-L. Wang, C.-H. Hung, and E. W.-G. Diau, *Angew. Chem.* **129**, 14007 (2017).
- <sup>97</sup>T. Yokoyama, T.-B. Song, D. H. Cao, C. C. Stoumpos, S. Aramaki, and M. G. Kanatzidis, *ACS Energy Lett.* **2**, 22 (2017).
- <sup>98</sup>X. Liu, Z. Yang, C.-C. Chueh, A. Rajagopal, S. T. Williams, Y. Sun, and A. K.-Y. Jen, *J. Mater. Chem. A* **4**, 17939 (2016).
- <sup>99</sup>Z. Zhang, L. Wang, A. Kumar Baranwal, S. Razyeh Sahamir, G. Kapil, Y. Sanehira, M. Akmal Kamarudin, K. Nishimura, C. Ding, D. Liu, Y. Li, H. Li, M. Chen, Q. Shen, T. S. Ripolles, J. Bisquert, and S. Hayase, *J. Energy Chem.* **71**, 604 (2022).
- <sup>100</sup>X. Jiang, F. Wang, Q. Wei, H. Li, Y. Shang, W. Zhou, C. Wang, P. Cheng, Q. Chen, L. Chen, and Z. Ning, *Nat. Commun.* **11**, 1245 (2020).
- <sup>101</sup>M. Chen, Q. Dong, F. T. Eickemeyer, Y. Liu, Z. Dai, A. D. Carl, B. Bahrami, A. H. Chowdhury, R. L. Grimm, Y. Shi, Q. Qiao, S. M. Zakeeruddin, M. Grätzel, and N. P. Padture, *ACS Energy Lett.* **5**, 2223 (2020).
- <sup>102</sup>T. Wu, X. Liu, X. He, Y. Wang, X. Meng, T. Noda, X. Yang, and L. Han, *Sci. China Chem.* **63**, 107 (2020).
- <sup>103</sup>F. Gu, S. Ye, Z. Zhao, H. Rao, Z. Liu, Z. Bian, and C. Huang, *Sol. RRL* **2**, 1800136 (2018).
- <sup>104</sup>Z. Zhao, F. Gu, Y. Li, W. Sun, S. Ye, H. Rao, Z. Liu, Z. Bian, and C. Huang, *Adv. Sci.* **4**, 1700204 (2017).
- <sup>105</sup>X. Meng, J. Lin, X. Liu, X. He, Y. Wang, T. Noda, T. Wu, X. Yang, and L. Han, *Adv. Mater.* **31**, 1903721 (2019).
- <sup>106</sup>W. Liao, D. Zhao, Y. Yu, C. R. Grice, C. Wang, A. J. Cimaroli, P. Schulz, W. Meng, K. Zhu, R. G. Xiong, and Y. Yan, *Adv. Mater.* **28**, 9333 (2016).
- <sup>107</sup>W. Ke, C. C. Stoumpos, J. L. Logsdon, M. R. Wasielewski, Y. Yan, G. Fang, and M. G. Kanatzidis, *J. Am. Chem. Soc.* **138**, 14998 (2016).
- <sup>108</sup>J. Xi, Z. Wu, B. Jiao, H. Dong, C. Ran, C. Piao, T. Lei, T. B. Song, W. Ke, T. Yokoyama, X. Hou, and M. G. Kanatzidis, *Adv. Mater.* **29**, 1606964 (2017).
- <sup>109</sup>T. M. Koh, T. Krishnamoorthy, N. Yantara, C. Shi, W. L. Leong, P. P. Boix, A. C. Grimsdale, S. G. Mhaisalkar, and N. Mathews, *J. Mater. Chem. A* **3**, 14996 (2015).
- <sup>110</sup>W. Gu, X. Xu, J. Chen, B. Ma, M. Qin, W. Zhu, J. Qian, Z. Qin, W. Shen, Y. Lu, W. Zhang, S. Chen, X. Lu, and W. Huang, *Sol. RRL* **4**, 2000153 (2020).
- <sup>111</sup>S. J. Lee, S. S. Shin, J. Im, T. K. Ahn, J. H. Noh, N. J. Jeon, S. I. Seok, and J. Seo, *ACS Energy Lett.* **3**, 46 (2017).
- <sup>112</sup>X. Liu, K. Yan, D. Tan, X. Liang, H. Zhang, and W. Huang, *ACS Energy Lett.* **3**, 2701 (2018).
- <sup>113</sup>J. Liu, M. Ozaki, S. Yakumaru, T. Handa, R. Nishikubo, Y. Kanemitsu, A. Saeki, Y. Murata, R. Murdey, and A. Wakamiya, *Angew. Chem.* **130**, 13405 (2018).
- <sup>114</sup>N. Ito, M. A. Kamarudin, D. Hirotani, Y. Zhang, Q. Shen, Y. Ogomi, S. Iikubo, T. Minemoto, K. Yoshino, and S. Hayase, *J. Phys. Chem. Lett.* **9**, 1682 (2018).
- <sup>115</sup>C. H. Ng, K. Nishimura, N. Ito, K. Hamada, D. Hirotani, Z. Wang, F. Yang, S. Iikubo, Q. Shen, K. Yoshino, T. Minemoto, and S. Hayase, *Nano Energy* **58**, 130 (2019).
- <sup>116</sup>T.-B. Song, T. Yokoyama, S. Aramaki, and M. G. Kanatzidis, *ACS Energy Lett.* **2**, 897 (2017).
- <sup>117</sup>T.-B. Song, T. Yokoyama, J. Logsdon, M. R. Wasielewski, S. Aramaki, and M. G. Kanatzidis, *ACS Appl. Energy Mater.* **1**, 4221 (2018).
- <sup>118</sup>K. Marshall, M. Walker, R. Walton, and R. Hatton, *Nat. Energy* **1**, 16178 (2016).
- <sup>119</sup>N. Wang, Y. Zhou, M.-G. Ju, H. F. Garces, T. Ding, S. Pang, X. C. Zeng, N. P. Padture, and X. W. Sun, *Adv. Energy Mater.* **6**, 1601130 (2016).
- <sup>120</sup>K. P. Marshall, R. I. Walton, and R. A. Hatton, *J. Mater. Chem. A* **3**, 11631 (2015).
- <sup>121</sup>M. H. Kumar, S. Dharani, W. L. Leong, P. P. Boix, R. R. Prabhakar, T. Baikie, C. Shi, H. Ding, R. Ramesh, M. Asta, M. Graetzel, S. G. Mhaisalkar, and N. Mathews, *Adv. Mater.* **26**, 7122 (2014).
- <sup>122</sup>W. Li, J. Li, J. Li, J. Fan, Y. Mai, and L. Wang, *J. Mater. Chem. A* **4**, 17104 (2016).
- <sup>123</sup>S. Gupta, T. Bendikov, G. Hodes, and D. Cahen, *ACS Energy Lett.* **1**, 1028 (2016).
- <sup>124</sup>D. Moghe, L. Wang, C. J. Traverse, A. Redoute, M. Sponseller, P. R. Brown, V. Bulović, and R. R. Lunt, *Nano Energy* **28**, 469 (2016).
- <sup>125</sup>I. Kopacic, B. Friesenbichler, S. F. Hoefler, B. Kunert, H. Plank, T. Rath, and G. Trimmel, *ACS Appl. Energy Mater.* **1**, 343 (2018).
- <sup>126</sup>L.-J. Chen, *RSC Adv.* **8**, 18396 (2018).
- <sup>127</sup>T. Krishnamoorthy, H. Ding, C. Yan, W. L. Leong, T. Baikie, Z. Zhang, M. Sherburne, S. Li, M. Asta, N. Mathews, and S. G. Mhaisalkar, *J. Mater. Chem. A* **3**, 23829 (2015).
- <sup>128</sup>W. Ke, C. C. Stoumpos, I. Spanopoulos, L. Mao, M. Chen, M. R. Wasielewski, and M. G. Kanatzidis, *J. Am. Chem. Soc.* **139**, 14800 (2017).
- <sup>129</sup>B. Wang, N. Li, L. Yang, C. Dall'Agnese, A. K. Jena, S. Sasaki, T. Miyasaka, H. Tamiaki, and X.-F. Wang, *J. Am. Chem. Soc.* **143**, 2207 (2021).
- <sup>130</sup>X. Yang, Y. Chen, P. Liu, H. Xiang, W. Wang, R. Ran, W. Zhou, and Z. Shao, *Adv. Funct. Mater.* **30**, 2001557 (2020).
- <sup>131</sup>E. Greul, M. L. Petrus, A. Binek, P. Docampo, and T. Bein, *J. Mater. Chem. A* **5**, 19972 (2017).
- <sup>132</sup>C. Wu, Q. Zhang, Y. Liu, W. Luo, X. Guo, Z. Huang, H. Ting, W. Sun, X. Zhong, S. Wei, S. Wang, Z. Chen, and L. Xiao, *Adv. Sci.* **5**, 1700759 (2018).

- <sup>133</sup>P.-K. Kung, M.-H. Li, P.-Y. Lin, J.-Y. Jhang, M. Pantaler, D. C. Lupascu, G. Grancini, and P. Chen, *Sol. RRL* **4**, 1900306 (2020).
- <sup>134</sup>Z. Zhang, C. Wu, D. Wang, G. Liu, Q. Zhang, W. Luo, X. Qi, X. Guo, Y. Zhang, Y. Lao, B. Qu, L. Xiao, and Z. Chen, *Org. Electron.* **74**, 204 (2019).
- <sup>135</sup>C. Zhang, L. Gao, S. Teo, Z. Guo, Z. Xu, S. Zhao, and T. Ma, *Sustainable Energy Fuels* **2**, 2419 (2018).
- <sup>136</sup>E. M. Hutter, G. E. Eperon, S. D. Stranks, and T. J. Savenije, *J. Phys. Chem. Lett.* **6**, 3082 (2015).
- <sup>137</sup>X. Qiu, Y. Jiang, H. Zhang, Z. Qiu, S. Yuan, P. Wang, and B. Cao, *Phys. Status Solidi RRL* **10**, 587 (2016).
- <sup>138</sup>B. Lee, A. Krenselewski, S. I. Baik, D. N. Seidman, and R. P. H. Chang, *Sustainable Energy Fuels* **1**, 710 (2017).
- <sup>139</sup>Y. Jiang, H. Zhang, X. Qiu, and B. Cao, *Mater. Lett.* **199**, 50 (2017).
- <sup>140</sup>M. Chen, M.-G. Ju, A. D. Carl, Y. Zong, R. L. Grimm, J. Gu, X. C. Zeng, Y. Zhou, and N. P. Padture, *Joule* **2**, 558 (2018).
- <sup>141</sup>A. Kaltzoglou, M. Antoniadou, D. Perganti, E. Siranidi, V. Raptis, K. Trohidou, V. Psycharis, A. G. Kontos, and P. Falaras, *Electrochim. Acta* **184**, 466 (2015).
- <sup>142</sup>X. Zhang, G. Wu, Z. Gu, B. Guo, W. Liu, S. Yang, T. Ye, C. Chen, W. Tu, and H. Chen, *Nano Res.* **9**, 2921 (2016).
- <sup>143</sup>C. Ran, Z. Wu, J. Xi, F. Yuan, H. Dong, T. Lei, X. He, and X. Hou, *J. Phys. Chem. Lett.* **8**, 394 (2017).
- <sup>144</sup>S. S. Mali, H. Kim, D.-H. Kim, and C. Kook Hong, *ChemistrySelect* **2**, 1578 (2017).
- <sup>145</sup>A. Kulkarni, T. Singh, M. Ikegami, and T. Miyasaka, *RSC Adv.* **7**, 9456 (2017).
- <sup>146</sup>B.-W. Park, B. Philippe, X. Zhang, H. Rensmo, G. Boschloo, and E. M. J. Johansson, *Adv. Mater.* **27**, 6806 (2015).
- <sup>147</sup>M. Abulikemu, S. Ould-Chikh, X. Miao, E. Alarousu, B. Murali, G. O. Ngongang Ndjawa, J. Barbé, A. El Labban, A. Amassian, and S. Del Gobbo, *J. Mater. Chem. A* **4**, 12504 (2016).
- <sup>148</sup>T. Okano and Y. Suzuki, *Mater. Lett.* **191**, 77 (2017).
- <sup>149</sup>S. Öz, J.-C. Hebig, E. Jung, T. Singh, A. Lepcha, S. Olthof, F. Jan, Y. Gao, R. German, P. H. M. van Loosdrecht, K. Meerholz, T. Kirchartz, and S. Mathur, *Sol. Energy Mater. Sol. Cells* **158**, 195 (2016).
- <sup>150</sup>H. Li, C. Wu, Y. Yan, B. Chi, J. Pu, J. Li, and S. Priya, *ChemSusChem* **10**, 3994 (2017).
- <sup>151</sup>P. Karuppuswamy, K. M. Boopathi, A. Mohapatra, H.-C. Chen, K.-T. Wong, P.-C. Wang, and C.-W. Chu, *Nano Energy* **45**, 330 (2018).
- <sup>152</sup>K. M. Boopathi, P. Karuppuswamy, A. Singh, C. Hanmandlu, L. Lin, S. A. Abbas, C. C. Chang, P. C. Wang, G. Li, and C. W. Chu, *J. Mater. Chem. A* **5**, 20843 (2017).
- <sup>153</sup>S. Chatterjee and A. J. Pal, *ACS Appl. Mater. Interfaces* **10**, 35194 (2018).
- <sup>154</sup>J.-C. Hebig, I. Kühn, J. Flohre, and T. Kirchartz, *ACS Energy Lett.* **1**, 309 (2016).
- <sup>155</sup>M. B. Johansson, H. Zhu, and E. M. J. Johansson, *J. Phys. Chem. Lett.* **7**, 3467 (2016).
- <sup>156</sup>P. C. Harikesh, H. K. Mulmudi, B. Ghosh, T. W. Goh, Y. T. Teng, K. Thirumal, M. Lockrey, K. Weber, T. M. Koh, S. Li, S. Mhaisalkar, and N. Mathews, *Chem. Mater.* **28**, 7496 (2016).
- <sup>157</sup>C. Zuo and L. Ding, *Angew. Chem.* **129**, 6628 (2017).
- <sup>158</sup>A. Rajagopal, R. J. Stoddard, H. W. Hillhouse, and A. K.-Y. Jen, *J. Mater. Chem. A* **7**, 16285 (2019).
- <sup>159</sup>T. Luo, Y. Xia, J. Huang, X. Huang, Z. Wu, Y. Chen, X. Xu, W. Xie, P. Liu, C. Hu, X. Lu, and T. Shi, *CrystEngComm* **23**, 4917 (2021).
- <sup>160</sup>J. Chang, L. Jiang, G. Wang, W. Zhao, Y. Huang, and H. Chen, *Phys. Chem. Chem. Phys.* **23**, 14449 (2021).
- <sup>161</sup>Y. Raoui, S. Kazim, Y. Galagan, H. Ez-Zahraouy, and S. Ahmad, *Sustainable Energy Fuels* **5**, 4661 (2021).
- <sup>162</sup>L. Schade, S. Mahesh, G. Volonakis, M. Zacharias, B. Wenger, F. Schmidt, S. V. Kesava, D. Prabhakaran, M. Abdi-Jalebi, M. Lenz, F. Giustino, G. Longo, P. G. Radaelli, and H. J. Snaith, *ACS Energy Lett.* **6**, 1073 (2021).
- <sup>163</sup>Q. Zhou, Z. Bai, W.-g. Lu, Y. Wang, B. Zou, and H. Zhong, *Adv. Mater.* **28**, 9163 (2016).
- <sup>164</sup>C. Cho, B. Zhao, G. D. Tainter, J.-Y. Lee, R. H. Friend, D. Di, F. Deschler, and N. C. Greenham, *Nat. Commun.* **11**, 611 (2020).
- <sup>165</sup>Z. Liu, W. Qiu, X. Peng, G. Sun, X. Liu, D. Liu, Z. Li, F. He, C. Shen, Q. Gu, F. Ma, H. L. Yip, L. Hou, Z. Qi, and S. J. Su, *Adv. Mater.* **33**, 2103268 (2021).
- <sup>166</sup>H. Tsai, S. Shrestha, R. A. Vilá, W. Huang, C. Liu, C.-H. Hou, H.-H. Huang, X. Wen, M. Li, G. Wiederrecht, Y. Cui, M. Cotlet, X. Zhang, X. Ma, and W. Nie, *Nat. Photonics* **15**, 843 (2021).
- <sup>167</sup>Y. Dong, Y.-K. Wang, F. Yuan, A. Johnston, Y. Liu, D. Ma, M.-J. Choi, B. Chen, M. Chekini, S.-W. Baek, L. K. Sagar, J. Fan, Y. Hou, M. Wu, S. Lee, B. Sun, S. Hoogland, R. Quintero-Bermudez, H. Ebe, P. Todorovic, F. Dinic, P. Li, H. T. Kung, M. I. Saidaminov, E. Kumacheva, E. Spiecker, L.-S. Liao, O. Voznyy, Z.-H. Lu, and E. H. Sargent, *Nat. Nanotechnol.* **15**, 668 (2020).
- <sup>168</sup>Z. Zhu, Y. Wu, Y. Shen, J. Tan, D. Shen, M.-F. Lo, M. Li, Y. Yuan, J.-X. Tang, W. Zhang, S.-W. Tsang, Z. Guan, and C.-S. Lee, *Chem. Mater.* **33**, 4154 (2021).
- <sup>169</sup>H. Xiang, R. Wang, J. Chen, F. Li, and H. Zeng, *Light: Sci. Appl.* **10**, 206 (2021).
- <sup>170</sup>R. Sun, P. Lu, D. Zhou, W. Xu, N. Ding, H. Shao, Y. Zhang, D. Li, N. Wang, X. Zhuang, B. Dong, X. Bai, and H. Song, *ACS Energy Lett.* **5**, 2131 (2020).
- <sup>171</sup>K. Zhang, N. Zhu, M. Zhang, L. Wang, and J. Xing, *J. Mater. Chem. C* **9**, 3795 (2021).
- <sup>172</sup>L. Protesescu, S. Yakunin, M. I. Bodnarchuk, F. Krieg, R. Caputo, C. H. Hendon, R. X. Yang, A. Walsh, and M. V. Kovalenko, *Nano Lett.* **15**, 3692 (2015).
- <sup>173</sup>Y.-H. Kim, H. Cho, J. H. Heo, T.-S. Kim, N. Myoung, C.-L. Lee, S. H. Im, and T.-W. Lee, *Adv. Mater.* **27**, 1248 (2015).
- <sup>174</sup>J. Song, J. Li, X. Li, L. Xu, Y. Dong, and H. Zeng, *Adv. Mater.* **27**, 7162 (2015).
- <sup>175</sup>B. Ke, R. Zeng, Z. Zhao, Q. Wei, X. Xue, K. Bai, C. Cai, W. Zhou, Z. Xia, and B. Zou, *J. Phys. Chem. Lett.* **11**, 340 (2020).
- <sup>176</sup>P. Han, X. Mao, S. Yang, F. Zhang, B. Yang, D. Wei, W. Deng, and K. Han, *Angew. Chem.* **131**, 17391 (2019).
- <sup>177</sup>J. Luo, X. Wang, S. Li, J. Liu, Y. Guo, G. Niu, L. Yao, Y. Fu, L. Gao, Q. Dong, C. Zhao, M. Leng, F. Ma, W. Liang, L. Wang, S. Jin, J. Han, L. Zhang, J. Etheridge, J. Wang, Y. Yan, E. H. Sargent, and J. Tang, *Nature* **563**, 541 (2018).
- <sup>178</sup>K. z. Du, W. Meng, X. Wang, Y. Yan, and D. B. Mitzi, *Angew. Chem., Int. Ed.* **56**, 8158 (2017).
- <sup>179</sup>T. T. Tran, J. R. Panella, J. R. Chamorro, J. R. Morey, and T. M. McQueen, *Mater. Horiz.* **4**, 688 (2017).
- <sup>180</sup>F. Locardi, M. Cirignano, D. Baranov, Z. Dang, M. Prato, F. Drago, M. Ferretti, V. Pinchetti, M. Fanciulli, S. Brovelli, L. De Trizio, and L. Manna, *J. Am. Chem. Soc.* **140**, 12989 (2018).
- <sup>181</sup>J. D. Majher, M. B. Gray, T. A. Strom, and P. M. Woodward, *Chem. Mater.* **31**, 1738 (2019).
- <sup>182</sup>C.-Y. Wang, P. Liang, R.-J. Xie, Y. Yao, P. Liu, Y. Yang, J. Hu, L. Shao, X. W. Sun, F. Kang, and G. Wei, *Chem. Mater.* **32**, 7814 (2020).
- <sup>183</sup>M. Hu, J. Luo, S. Li, J. Liu, J. Li, Z. Tan, G. Niu, Z. Wang, and J. Tang, *Opt. Lett.* **44**, 4757 (2019).
- <sup>184</sup>G. Zhou, X. Jiang, M. Molokeev, Z. Lin, J. Zhao, J. Wang, and Z. Xia, *Chem. Mater.* **31**, 5788 (2019).
- <sup>185</sup>A. Noculak, V. Morad, K. M. McCall, S. Yakunin, Y. Shynkarenko, M. Wörle, and M. V. Kovalenko, *Chem. Mater.* **32**, 5118 (2020).
- <sup>186</sup>Z. Tan, Y. Chu, J. Chen, J. Li, G. Ji, G. Niu, L. Gao, Z. Xiao, and J. Tang, *Adv. Mater.* **32**, 2002443 (2020).
- <sup>187</sup>Z. Li, C. Zhang, B. Li, C. Lin, Y. Li, L. Wang, and R.-J. Xie, *Chem. Eng. J.* **420**, 129740 (2021).
- <sup>188</sup>A. Wang, Y. Guo, F. Muhammad, and Z. Deng, *Chem. Mater.* **29**, 6493 (2017).
- <sup>189</sup>A. B. Wong, Y. Bekenstein, J. Kang, C. S. Kley, D. Kim, N. A. Gibson, D. Zhang, Y. Yu, S. R. Leone, L.-W. Wang, A. P. Alivisatos, and P. Yang, *Nano Lett.* **18**, 2060 (2018).
- <sup>190</sup>F. Yuan, J. Xi, H. Dong, K. Xi, W. Zhang, C. Ran, B. Jiao, X. Hou, A. K.-Y. Jen, and Z. Wu, *Phys. Status Solidi RRL* **12**, 1800090 (2018).
- <sup>191</sup>W.-L. Hong, Y.-C. Huang, C.-Y. Chang, Z.-C. Zhang, H.-R. Tsai, N.-Y. Chang, and Y.-C. Chao, *Adv. Mater.* **28**, 8029 (2016).
- <sup>192</sup>Z. Yang, Z. Jiang, X. Liu, X. Zhou, J. Zhang, and W. Li, *Adv. Opt. Mater.* **7**, 1900108 (2019).
- <sup>193</sup>B. Yang, J. Chen, S. Yang, F. Hong, L. Sun, P. Han, T. Pullerits, W. Deng, and K. Han, *Angew. Chem.* **130**, 5457 (2018).
- <sup>194</sup>S. Li, Q. Hu, J. Luo, T. Jin, J. Liu, J. Li, Z. Tan, Y. Han, Z. Zheng, T. Zhai, H. Song, L. Gao, G. Niu, and J. Tang, *Adv. Opt. Mater.* **7**, 1901098 (2019).

- <sup>195</sup>P. Han, X. Zhang, X. Mao, B. Yang, S. Yang, Z. Feng, D. Wei, W. Deng, T. Pullerits, and K. Han, *Sci. China Chem.* **62**, 1405 (2019).
- <sup>196</sup>F. Locardi, E. Sartori, J. Buha, J. Zito, M. Prato, V. Pinchetti, M. L. Zaffalon, M. Ferretti, S. Brovelli, I. Infante, L. De Trizio, and L. Manna, *ACS Energy Lett.* **4**, 1976 (2019).
- <sup>197</sup>A. Karmakar, G. M. Bernard, A. Meldrum, A. O. Oliyynyk, and V. K. Michaelis, *J. Am. Chem. Soc.* **142**, 10780 (2020).
- <sup>198</sup>F. Zhao, Z. Song, J. Zhao, and Q. Liu, *Inorg. Chem. Front.* **6**, 3621 (2019).
- <sup>199</sup>K. N. Nandha and A. Nag, *Chem. Commun.* **54**, 5205 (2018).
- <sup>200</sup>Q. Hu, Z. Deng, M. Hu, A. Zhao, Y. Zhang, Z. Tan, G. Niu, H. Wu, and J. Tang, *Sci. China Chem.* **61**, 1581 (2018).
- <sup>201</sup>Z. Tan, J. Li, C. Zhang, Z. Li, Q. Hu, Z. Xiao, T. Kamiya, H. Hosono, G. Niu, E. Lifshitz, Y. Cheng, and J. Tang, *Adv. Funct. Mater.* **28**, 1801131 (2018).
- <sup>202</sup>J. Li, Z. Tan, M. Hu, C. Chen, J. Luo, S. Li, L. Gao, Z. Xiao, G. Niu, and J. Tang, *Front. Optoelectron.* **12**, 352 (2019).
- <sup>203</sup>H. Zhang, L. Zhu, J. Cheng, L. Chen, C. Liu, and S. Yuan, *Materials* **12**, 1501 (2019).
- <sup>204</sup>B. M. Benin, D. N. Dirin, V. Morad, M. Wörle, S. Yakunin, G. Rainò, O. Nazarenko, M. Fischer, I. Infante, and M. V. Kovalenko, *Angew. Chem., Int. Ed.* **57**, 11329 (2018).
- <sup>205</sup>G. Xiong, L. Yuan, Y. Jin, H. Wu, Z. Li, B. Qu, G. Ju, L. Chen, S. Yang, and Y. Hu, *Adv. Opt. Mater.* **8**, 2000779 (2020).
- <sup>206</sup>M. Leng, Y. Yang, K. Zeng, Z. Chen, Z. Tan, S. Li, J. Li, B. Xu, D. Li, M. P. Hautzinger, Y. Fu, T. Zhai, L. Xu, G. Niu, S. Jin, and J. Tang, *Adv. Funct. Mater.* **28**, 1704446 (2018).
- <sup>207</sup>Z. Ma, Z. Shi, D. Yang, F. Zhang, S. Li, L. Wang, D. Wu, Y. Zhang, G. Na, L. Zhang, X. Li, Y. Zhang, and C. Shan, *ACS Energy Lett.* **5**, 385 (2020).
- <sup>208</sup>Y. Shen, J. Yin, B. Cai, Z. Wang, Y. Dong, X. Xu, and H. Zeng, *Nanoscale Horiz.* **5**, 580 (2020).
- <sup>209</sup>M. Leng, Z. Chen, Y. Yang, Z. Li, K. Zeng, K. Li, G. Niu, Y. He, Q. Zhou, and J. Tang, *Angew. Chem., Int. Ed.* **55**, 15012 (2016).
- <sup>210</sup>M. Leng, Y. Yang, Z. Chen, W. Gao, J. Zhang, G. Niu, D. Li, H. Song, J. Zhang, S. Jin, and J. Tang, *Nano Lett.* **18**, 6076 (2018).
- <sup>211</sup>E. Gong, S. Ali, C. B. Hiragond, H. S. Kim, N. S. Powar, D. Kim, H. Kim, and S.-I. In, *Energy Environ. Sci.* **15**, 880 (2022).
- <sup>212</sup>K. Ren, S. Yue, C. Li, Z. Fang, K. A. M. Gasem, J. Leszczynski, S. Qu, Z. Wang, and M. Fan, *J. Mater. Chem. A* **10**, 407 (2022).
- <sup>213</sup>S. Purohit, K. L. Yadav, and S. Satapathi, *Adv. Mater. Interfaces* **9**, 2200058 (2022).
- <sup>214</sup>H. Huang, B. Weng, H. Zhang, F. Lai, J. Long, J. Hofkens, R. E. Douthwaite, J. A. Steele, and M. B. J. Roeffaers, *J. Phys. Chem. Lett.* **13**, 25 (2022).
- <sup>215</sup>O. Khaselev and J. A. Turner, *Science* **280**, 425 (1998).
- <sup>216</sup>M. M. May, H.-J. Lewerenz, D. Lackner, F. Dimroth, and T. Hannappel, *Nat. Commun.* **6**, 8286 (2015).
- <sup>217</sup>J. Jia, L. C. Seitz, J. D. Benck, Y. Huo, Y. Chen, J. W. D. Ng, T. Bilir, J. S. Harris, and T. F. Jaramillo, *Nat. Commun.* **7**, 13237 (2016).
- <sup>218</sup>W.-H. Cheng, M. H. Richter, M. M. May, J. Ohlmann, D. Lackner, F. Dimroth, T. Hannappel, H. A. Atwater, and H.-J. Lewerenz, *ACS Energy Lett.* **3**, 1795 (2018).
- <sup>219</sup>J. Tournet, Y. Lee, S. K. Karuturi, H. H. Tan, and C. Jagadish, *ACS Energy Lett.* **5**, 611 (2020).
- <sup>220</sup>J. Gao, F. Sahli, C. Liu, D. Ren, X. Guo, J. Werner, Q. Jeangros, S. M. Zakeeruddin, C. Ballif, M. Grätzel, and J. Luo, *Joule* **3**, 2930 (2019).
- <sup>221</sup>S. Park, W. J. Chang, C. W. Lee, S. Park, H.-Y. Ahn, and K. T. Nam, *Nat. Energy* **2**, 16185 (2017).
- <sup>222</sup>X. Wang, H. Wang, H. Zhang, W. Yu, X. Wang, Y. Zhao, X. Zong, and C. Li, *ACS Energy Lett.* **3**, 1159 (2018).
- <sup>223</sup>H. Wang, X. Wang, R. Chen, H. Zhang, X. Wang, J. Wang, J. Zhang, L. Mu, K. Wu, F. Fan, X. Zong, and C. Li, *ACS Energy Lett.* **4**, 40 (2019).
- <sup>224</sup>Y.-F. Xu, M.-Z. Yang, B.-X. Chen, X.-D. Wang, H.-Y. Chen, D.-B. Kuang, and C.-Y. Su, *J. Am. Chem. Soc.* **139**, 5660 (2017).
- <sup>225</sup>G. Volonakis and F. Giustino, *Appl. Phys. Lett.* **112**, 243901 (2018).
- <sup>226</sup>D. Wu, X. Zhao, Y. Huang, J. Lai, H. Li, J. Yang, C. Tian, P. He, Q. Huang, and X. Tang, *Chem. Mater.* **33**, 4971 (2021).
- <sup>227</sup>D. Wu, X. Zhao, Y. Huang, J. Lai, J. Yang, C. Tian, P. He, Q. Huang, and X. Tang, *J. Phys. Chem. C* **125**, 18328 (2021).
- <sup>228</sup>Z. Liu, H. Yang, J. Wang, Y. Yuan, K. Hills-Kimball, T. Cai, P. Wang, A. Tang, and O. Chen, *Nano Lett.* **21**, 1620 (2021).
- <sup>229</sup>G. Zhang, A. Chaves, S. Huang, F. Wang, Q. Xing, T. Low, and H. Yan, *Sci. Adv.* **4**, eaap9977 (2018).
- <sup>230</sup>T. Otterburg, D. Y. Oberli, M.-A. Dupertuis, N. Moret, E. Pelucchi, B. Dwir, K. Leifer, and E. Kapon, *Phys. Rev. B* **71**, 033301 (2005).
- <sup>231</sup>K. Zheng, Q. Zhu, M. Abdellah, M. E. Messing, W. Zhang, A. Generalov, Y. Niu, L. Ribaud, S. E. Canton, and T. Pullerits, *J. Phys. Chem. Lett.* **6**, 2969 (2015).
- <sup>232</sup>Y. Jiang, K. Li, X. Wu, M. Zhu, H. Zhang, K. Zhang, Y. Wang, K. P. Loh, Y. Shi, and Q.-H. Xu, *ACS Appl. Mater. Interfaces* **13**, 10037 (2021).
- <sup>233</sup>C. Lu, D. S. Itanze, A. G. Aragon, X. Ma, H. Li, K. B. Ucer, C. Hewitt, D. L. Carroll, R. T. Williams, Y. Qiu, and S. M. Geyer, *Nanoscale* **12**, 2987 (2020).
- <sup>234</sup>L. Romani, A. Speltini, F. Ambrosio, E. Mosconi, A. Profumo, M. Marelli, S. Margadonna, A. Milella, F. Fracassi, A. Listorti, F. De Angelis, and L. Malavasi, *Angew. Chem., Int. Ed.* **60**, 3611 (2021).
- <sup>235</sup>Y. Q. Gao, Y. Georgievskii, and R. A. Marcus, *J. Chem. Phys.* **112**, 3358 (2000).
- <sup>236</sup>K. Li, S. Li, W. Zhang, Z. Shi, D. Wu, X. Chen, P. Lin, Y. Tian, and X. Li, *J. Colloid Interface Sci.* **596**, 376 (2021).
- <sup>237</sup>D. Wu, Y. Tao, Y. Huang, B. Huo, X. Zhao, J. Yang, X. Jiang, Q. Huang, F. Dong, and X. Tang, *J. Catal.* **397**, 27 (2021).
- <sup>238</sup>Z. Zhang, Y. Liang, H. Huang, X. Liu, Q. Li, L. Chen, and D. Xu, *Angew. Chem., Int. Ed.* **58**, 7263 (2019).
- <sup>239</sup>Z. Zhang, Y. Yang, Y. Wang, L. Yang, Q. Li, L. Chen, and D. Xu, *Angew. Chem.* **132**, 18293 (2020).
- <sup>240</sup>D. Ju, X. Zheng, J. Liu, Y. Chen, J. Zhang, B. Cao, H. Xiao, O. F. Mohammed, O. M. Bakr, and X. Tao, *Angew. Chem.* **130**, 15084 (2018).
- <sup>241</sup>A. Pisanu, A. Speltini, P. Quadrelli, G. Drera, L. Sangaletti, and L. Malavasi, *J. Mater. Chem. C* **7**, 7020 (2019).
- <sup>242</sup>L. Zhou, Y.-F. Xu, B.-X. Chen, D.-B. Kuang, and C.-Y. Su, *Small* **14**, 1703762 (2018).
- <sup>243</sup>Y. Wang, H. Huang, Z. Zhang, C. Wang, Y. Yang, Q. Li, and D. Xu, *Appl. Catal., B* **282**, 119570 (2021).
- <sup>244</sup>T. Wang, D. Yue, X. Li, and Y. Zhao, *Appl. Catal., B* **268**, 118399 (2020).
- <sup>245</sup>Z. He, Q. Tang, X. Liu, X. Yan, K. Li, and D. Yue, *Energy Fuels* **35**, 15005 (2021).
- <sup>246</sup>Y. Hai, W. Huang, Z. Li, D. Wu, Q. Huang, and X. Tang, *ACS Appl. Energy Mater.* **4**, 5913 (2021).
- <sup>247</sup>Y. Wang, Q. Zhou, Y. Zhu, and D. Xu, *Appl. Catal., B* **294**, 120236 (2021).
- <sup>248</sup>J. Sheng, Y. He, J. Li, C. Yuan, H. Huang, S. Wang, Y. Sun, Z. Wang, and F. Dong, *ACS Nano* **14**, 13103 (2020).
- <sup>249</sup>S. S. Bhosale, A. K. Kharade, E. Jocar, A. Fathi, S.-m. Chang, and E. W.-G. Diau, *J. Am. Chem. Soc.* **141**, 20434 (2019).
- <sup>250</sup>Y.-Y. Wang, X.-Y. Ji, M. Yu, and J. Tao, *Mater. Chem. Front.* **5**, 7796 (2021).
- <sup>251</sup>Y. Guo, G. Liu, Z. Li, Y. Lou, J. Chen, and Y. Zhao, *ACS Sustainable Chem. Eng.* **7**, 15080 (2019).
- <sup>252</sup>G. Chen, P. Wang, Y. Wu, Q. Zhang, Q. Wu, Z. Wang, Z. Zheng, Y. Liu, Y. Dai, and B. Huang, *Adv. Mater.* **32**, 2001344 (2020).
- <sup>253</sup>J. Tong, Z. Song, D. H. Kim, X. Chen, C. Chen, A. F. Palmstrom, P. F. Ndione, M. O. Reese, S. P. Dunfield, O. G. Reid, J. Liu, F. Zhang, S. P. Harvey, Z. Li, S. T. Christensen, G. Teeter, D. Zhao, M. M. Al-Jassim, M. F. A. M. van Hest, M. C. Beard, S. E. Shaheen, J. J. Berry, Y. Yan, and K. Zhu, *Science* **364**, 475 (2019).
- <sup>254</sup>S. R. Sahamir, M. A. Kamarudin, T. S. Ripolles, A. K. Baranwal, G. Kapil, Q. Shen, H. Segawa, J. Bisquert, and S. Hayase, *J. Phys. Chem. Lett.* **13**, 3130 (2022).